https://doi.org/10.5194/egusphere-2026-4735
Preprint. Discussion started: 9 September 2026

From in situ to remote sensing: a framework for quantifying boundary-condition sensitivity in soil organic carbon models across diverse European sites

Yue Zhou[1], Maria Costanza Andrenelli[2], Quentin Beauclaire[6], Eyal Ben-Dor [11], Sara Bergante[13], Javier Bravo-García[3], David de la Fuente Blanco[5], Asa Gholizadeh[4], David Čejka[4], Sabine Chabrillat[8,12], Bernard Heinesch[6], Laura Hernandez Mateo[16], Kevin Kuehl[15], Bernard Longdoz[6], Carlos Lozano Fondón[2], Petr Maca[4], Robert Milewski[8], Stefano Monaco[14], Dimitra Palantza[9], Francesco Palazzi[14], Maria Fantappiè[2], Roberta Farina[2], Marmar Sabetizadeh[10], Benjamin Sanchez[7], Inés Santín[7], Jonti Evan Shepherd[11], Judit Torres[16], Marta Gómez-Giménez[5], Bas van Wesemael[10], Bertrand Guenet[1*]

[1] Laboratoire de Géologie, École Normale Supérieure (ENS), CNRS, Paris, France.
[2] Research Centre for Agriculture and Environment, Consiglio per la Ricerca in Agricoltura e l'Analisi dell'Economia Agraria (CREA-AA), via di Lanciola 12/A, Cascine del Riccio, Florence, Italy.
[3]Evenor-Tech, Seville, Spain.
[4] Department of Soil Science and Soil Protection, Faculty of Agrobiology, Food and Natural Resources, Czech University of Life Sciences Prague, Kamycka 129, Prague, 16500, Czech Republic.
[5]Remote Sensing & Geospatial Analytics, GMV, Isaac Newton 11, 28760, Tres Cantos, Spain.
[6]BIODYNE Biosystems Dynamics and Exchanges, TERRA Teaching and Research Center, Gembloux Agro-Bio Tech, University of Liege, Liege, Belgium.
[7]National Centre for Agricultural and Food Research and Technology, INIA-CSIC, Ctra. La Coruña km 7.5. 28040, Madrid, Spain.
[8]GFZ Helmholtz-Zentrum für Geoforschung, Potsdam, Germany.
[9]Aristotle University of Thessaloniki, Greece, Lab of Remote Sensing Spectroscopy and GIS, School of Agriculture.
[10]Earth and Life Institute, Université catholique de Louvain (UCLouvain), Louvain-la-Neuve, Belgium.
[11]The Remote Sensing Laboratory, Department of Geophysics, Faculty of Exact Sciences, Tel Aviv University, Tel Aviv-Yafo, Israel.
[12]Institute of Soil Science, Leibniz University Hannover, Hannover, Germany.
[13]Research Centre for Forestry and Wood, Consiglio per la Ricerca in Agricoltura e l'Analisi dell'Economia Agraria (CREA-FL), Arezzo, Italy.
[14]Research Centre for Engineering and Agro-Food Processing, Consiglio per la Ricerca in Agricoltura e l'Analisi dell'Economia Agraria (CREA-IT), Strada delle Cacce 73, 10135 Turin, Italy.
[15]German Aerospace Center (DLR), Earth Observation Center (EOC), Weßling, Germany.
[16]Institute of Forest Science (ICIFOR), INIA-CSIC, Ctra. La Coruña km 7.5. 28040, Madrid, Spain

Correspondence to: Bertrand Guenet (guenet@geologie.ens.fr)

Abstract. Process-based soil organic carbon (SOC) models are widely used for carbon accounting and assessments. For applications beyond experimental sites, remote sensing–derived inputs are often used to complement or replace in situ boundary conditions. This substitution introduces additional sensitivity that has rarely been explicitly quantified. Here, we propose a general framework to quantify boundary-condition sensitivity in SOC modelling, distinguishing between dynamic

https://doi.org/10.5194/egusphere-2026-4735
Preprint. Discussion started: 9 September 2026

sensitivity, which reflects deviations in the temporal trajectory of SOC stocks, and endpoint sensitivity, which captures differences in estimated SOC changes over defined reporting periods. Sensitivity is quantified by comparing substitution simulations, in which boundary conditions are replaced one by one with remote sensing–derived spatial datasets, against a baseline simulation driven by in situ observations. The framework is applied to 16 long-term experimental sites across Europe, covering diverse land-use types and environmental conditions.

Boundary-condition substitution affected both SOC trajectories and endpoint estimates, although the magnitude and form of these effects varied among inputs. Initial SOC, vegetation-derived carbon inputs, and climate data were the dominant drivers of dynamic sensitivity. Fixed endpoint sensitivity was generally small relative to measured SOC changes, supporting the use of remote sensing–derived spatial datasets as scalable boundary-condition proxies for SOC modelling. Rolling endpoint sensitivity further revealed that SOC change assessments depend not only on SOC dynamics but also on the selected reporting window. Short reporting periods were more affected by short-term variability, whereas longer periods were more susceptible to accumulated deviations. A reporting window of approximately 15–30 years provided a practical balance between these effects.

Overall, the framework enables a systematic quantification of sensitivity arising from boundary-condition substitution, enabling evaluation of both trajectory and reporting robustness. These findings highlight the importance of jointly considering critical boundary conditions and reporting-window design when applying remote sensing–driven SOC modelling for regional carbon accounting.

1 Introduction

Soil organic carbon (SOC) stocks and their temporal dynamics play a vital role in the global carbon cycle and constitute a key component of national and regional greenhouse gas accounting frameworks (Lal, 2004; Paustian et al., 2016). Accurate quantification of SOC changes is therefore essential for assessing mitigation potentials and supporting climate policy, particularly within Land-Use, Land-Use Change and Forestry (LULUCF) reporting (IPCC, 2006; Minasny et al., 2017).

Process-based soil carbon models are widely used to simulate SOC dynamics under varying climate and management scenarios and to support carbon accounting at multiple spatial scales (FAO, 2020; Wiesmeier et al., 2016; Morais et al., 2019). However, these models are data-intensive, requiring detailed and consistent information on climate, soil properties, vegetation, and/or management practices (Wiltshire et al., 2024; Ellis & Paustian, 2024). At the site scale, long-term experimental studies provide high-quality in situ observations that are indispensable for model development, calibration, and evaluation (Smith et al., 2020). Despite the large diversity of SOC models developed over past decades (Le Noë et al., 2023), their performance is generally robust when properly calibrated and constrained by site-specific observations, although the best-performing model often depends on local environmental conditions (Bruni et al., 2024). However, such high-quality observations remain point-based and unevenly distributed, and cannot adequately support SOC modelling at regional to continental scales (Smith et al., 2020).

https://doi.org/10.5194/egusphere-2026-4735
Preprint. Discussion started: 9 September 2026

Consequently, upscaling SOC modelling beyond experimental sites is necessary but remains challenging, largely because long-term, large-scale in situ observations are scarce. As a result, model applications typically rely on spatialized datasets derived from Earth observation, Digital Soil Mapping (DSM), climate reanalysis products, statistical inventories, and other remote sensing (RS) products. Thus, spatial datasets become the primary and indispensable sources for providing necessary boundary conditions (e.g. climate, soil properties, vegetation characteristics, and management practices) for process-based soil carbon models (Smith et al., 2020). The substitution of in situ measurements with RS-derived inputs is therefore an unavoidable step when upscaling SOC simulations beyond experimental sites.

However, discrepancies between RS-derived inputs and field measurements are inevitable, meaning that errors are inevitably introduced during this substitution step. Differences between local observations and large-scale spatial datasets arise from multiple sources. First, errors inherent to RS products arise from atmospheric effects, sensor-related uncertainties, retrieval algorithm uncertainties, spatial aggregation effects, temporal mismatches, and modelling assumptions embedded within derived products (Choi et al., 2025; Tran et al., 2023; Wu and Li, 2009; Angelopoulou et al., 2019). Second, several key boundary conditions required by SOC models are not directly observable from space and therefore must be inferred using auxiliary data and modelling approaches, such as management-related variables (Zhou et al., 2025; Castaldi et al., 2026). Similarly, many contemporary SOC and soil property maps are generated either using Digital Soil Mapping (DSM) approaches (McBratney et al., 2003), which establish quantitative relationships between laboratory measurements and environmental covariates (e.g. terrain attributes, climate variables, and remote sensing indicators), or using Multi/Hyperspectral Remote Sensing (MRS) approaches based solely on optical RS data (Van Wesemael et al., 2024; Chabrillat et al., 2019), both typically using machine-learning algorithms. Critically, these deviations do not manifest as a single, uniform effect. Different boundary-condition substitutions may induce fundamentally different error structures, ranging from systematic offsets in simulated SOC levels to changes in the temporal trajectory of SOC dynamics. Such effects can alter temporal evolution of SOC stocks and, in some cases, influence conclusions regarding whether a system functions as a carbon source or a carbon sink. This issue is particularly critical in the context of SOC change reporting. In many modelling-based assessments, simulation periods are determined by data availability (Lai et al., 2026), reporting conventions (FAO, 2020), or targeted end years (Morais et al., 2019), and there is currently no universally accepted standard regarding the length of the simulation period. SOC changes or carbon sequestration rates are most commonly quantified using endpoint differences over fixed reporting windows (typically several decades). For example, simulation periods range from 20 years in the global GSOCseq project (FAO, 2020) to 30 years in the UK (Jordon et al., 2022), increasing to 40 years for Chinese croplands (Lin et al., 2024) and 100 years for Global croplands (Poeplau & Dechow, 2023). When deviations introduced by boundary-condition substitution are not explicitly considered, such endpoint-based SOC assessments may become highly sensitive to both the choice of input data sources and reporting period, which may even reverse the inferred direction of SOC change. Despite their potential implications for carbon accounting and monitoring, the different error structures arising from boundary-condition substitution have rarely been systematically and explicitly evaluated to date, resulting in an important knowledge gap regarding the robustness and scalability of process-based soil carbon models.

https://doi.org/10.5194/egusphere-2026-4735
Preprint. Discussion started: 9 September 2026

Here, we refer to the effects arising from the substitution of in situ boundary conditions with RS-derived inputs as boundary-condition sensitivity. We therefore propose a framework to evaluate this sensitivity in SOC modelling using Roth C process-based model. We distinguish between two dimensions of sensitivity: (i) dynamic sensitivity, which characterises deviations in the temporal evolution of SOC, and (ii) endpoint sensitivity, which captures differences in SOC change estimates over defined reporting periods. The framework is applied to a diverse network of long-term experimental sites spanning multiple European countries and land-use types, covering a wide range of SOC levels, climatic conditions, and management histories.

The specific objectives of this study are to:

(1) develop a systematic framework to quantify dynamic and endpoint sensitivity arising from the substitution of in-situ boundary conditions with RS–derived inputs.

(2) compare the magnitude and error structures of sensitivity associated with different boundary-condition substitutions and identify the most influential drivers.

(3) assess how sensitivity patterns vary across land-use types and regions.

(4) evaluate the influence of sensitivity on endpoint-based SOC assessments in the context of carbon accounting and monitoring.

By explicitly evaluating both dynamic and endpoint sensitivity, this study aims to improve the transparency, robustness and interpretability of SOC modelling approaches that rely on remote sensing inputs for large-scale carbon assessment and monitoring.

2 Methods

2.1 Study sites and data sources

This study included 16 long-term experimental sites (Table 1) distributed across five European countries: Germany (DE), Italy (IT), Czech Republic (CZ), Belgium (BE) and Spain (ES). These sites are part of the Horizon Europe MRV4SOC project (https://mrv4soc.eu/), which aims to develop a monitoring, reporting, and verification (MRV) framework for soil carbon across European land systems. These sites cover multiple land-use types, including cropland, grassland, agroforestry, forest, forest plantation and shrubland systems, and span a wide range of climatic conditions, soil properties, baseline SOC stocks, management practices (Table 1). Forest plantations refer to managed forests, typically composed of monocultures of fast-growing tree species cultivated for timber or biomass production.

https://doi.org/10.5194/egusphere-2026-4735
Preprint. Discussion started: 9 September 2026

Table 1. Overview of the long-term experimental sites

ID	Coordinate	Site Name	Belong to	Climate	Practice	Sim_Start	Sim_End	Length	Soil Depth	SOC stock $t\cdot C\cdot ha^{-1}$	Site contact person
DE-Crop-01	(53.871433° N, 13.264086° E)	Demmin	TERENO	Temperate oceanic	Cereal crop rotation superficial disc-harrowing	2017-01	2024-12	8	30 cm	65-71	Robert Milewski (milewski@gfz.de)
IT-Crop-02	(43.9846651482° N, 11.3416695208° E)	Fagna Plot4	CREA-Agriculture and Environment LTE experiment	Temperate oceanic	Monoculture (Maize) superficial disc-harrowing	1996	2011	17	30 cm	40-44	Maria Fantappiè (maria.fantappie@crea.gov.it)
IT-Crop-03	(43.9841546781° N, 11.3416761507° E)	Fagna Plot14			Monoculture (Maize) deep ploughing	1996	2011	17	30 cm	37-41	Maria Fantappiè (maria.fantappie@crea.gov.it)
CZ-Crop-04	(50.105663° N, 13.844916° E)	Amálie	"Smart Landscape"	Temperate	Reduced tillage	2000-01	2024-12	25	30 cm	35-39	(Asa Gholizadeh (gholizadeh@af.czu.cz)
BE-Crop-05	(50.551389° N, 4.746111° E)	Lonzée	ICOS (BE-Lon)	Temperate oceanic	Regular crop rotation Conventional tillage	2007-07	2017-12	10	30 cm	36-43	Bernard Heinesch (benjamin.dumont@uliege.be)
IT-Crop-06	(45.142890° N, 10.111830° E)	ERSAF Till	ERSAF LTE	Temperate	30 cm deep ploughing	2019-01	2022-12	4	30 cm	47-54	Francesco Palazzi (francesco.palazzi@crea.gov.it)
IT-Crop-07	(45.143690° N, 10.109370° E)	ERSAF NoTill	ERSAF LTE	Temperate	No tillage	2019-01	2024-12	6	30 cm	42-47	Francesco Palazzi (francesco.palazzi@crea.gov.it)
BE-Grass-01	(50.311667° N, 4.967778° E)	Dorinne	ICOS (BE-Dor)	Temperate oceanic	permanent grassland Rotational grazing	2021-01	2024-12	4	30 cm	91-94	Bernard Longdoz (bernard.longdoz@uliege.be)
SP-Grass-02	(37.353409° N, 6.239161° W)	Guadiamar	Post-spill monitoring network	Mediterranean	organic amendment	2000-10	2025-02	25	20cm	36-52	Javier Bravo García (j.bravo@evenor-tech.com)
SP-Agrofor-01	(39.191429° N, 6.150648° W)	Extremadura	Spanish ICP and NFI Networks	Mediterranean	Agrosilvopastoralism	1991	2017	26	20 cm	13-177	Laura Hernandez (hernandez.laura@inia.csic.es)
IT-Agrofor-02	(45.128750° N, 8.524670° E)	PopFras	Resampled farm field	Temperate	Poplar groves and arable crops alternate	1994-01	2024-12	31	30 cm	27-40	Francesco Palazzi (francesco.palazzi@crea.gov.it)
CZ-Forest-01	(50.106446° N, 13.850583° E)	Amálie	"Smart Landscape"	Temperate	Conventional even-aged forestry	2000-01	2024-12	25	30 cm	36-45	Asa Gholizadeh (gholizadeh@af.czu.cz)
SP-Forest-02	(37.353409° N, 6.239161° W)	Guadiamar	Post-spill monitoring network	Mediterranean	Riparian forest	2000-10	2025-02	25	20cm	46-62	Javier Bravo García (j.bravo@evenor-tech.com)
IT-ForPlan-01	(45.146090 ° N, 8.517640 ° E)	Mezzi	Farm of CREA-Center for	Temperate	poplar grove with prolonged set-aside periods	1987-01	2024-12	38	30 cm	28-38	Francesco Palazzi (francesco.palazzi@crea.gov.it)

https://doi.org/10.5194/egusphere-2026-4735
Preprint. Discussion started: 9 September 2026

IT-ForPlan-02	(45.145260 ° N, 8.517120 ° E)	Mezzi	Forestry and Wood	Temperate	poplar grove with reduced or no set-aside periods	1988-01	2024-12	37	30 cm	24-38	Francesco Palazzi (francesco.palazzi@crea.gov.it)
SP-shrub-01	(37.353409° N, 6.239161° W)	Guadiamar	Post-spill monitoring network	Mediterranean	organic amendment	2000-10	2025-02	25	20cm	42-62	Javier Bravo García (j.bravo@evenor-tech.com)

135

https://doi.org/10.5194/egusphere-2026-4735
Preprint. Discussion started: 9 September 2026

SOC dynamics of these sites were simulated using the Rothamsted Carbon model (RothC; Coleman and Jenkinson, 1996) or its modified version RothC10_N (Farina et al., 2013), which accounts for drier soil condition. RothC model is one of the most widely used process-based SOC models for simulating SOC dynamics under varying environmental and management conditions owing to its relatively simple structure, modest data requirements, and robust performance across a wide range of ecosystems. RothC model represents SOC turnover through multiple conceptual pools with distinct decomposition rates, with decomposition processes regulated by boundary conditions, including climate drivers (e.g. temperature, precipitation, and open pan evaporation), soil properties (e.g. clay content), initial SOC stocks, and carbon inputs from vegetation and organic amendments.

A summary of in-situ and remote sensing–based data sources is provided in Table 2. Most study sites are equipped with eddy covariance (EC) systems and are part of established European observation networks. As a result, site-level meteorological variables were obtained directly from continuous in-situ observations. In addition, all sites provide in-situ measurements of soil properties (e.g. SOC stocks, SOC content and clay content) collected following site-specific sampling protocols, as well as detailed records of management practices and vegetation characteristics. For RS or RS-derived products, climate variables were directly obtained from open-access gridded datasets such as ERA5 (Hersbach et al., 2020), TerraClimate (Abatzoglou et al., 2018) and CHELSA (Karger et al., 2017). Soil properties (e.g. clay content and initial SOC stocks) were mainly derived from DSM or MRS approaches introduced above. Readily available products, such as SoilGrids (Poggio et al., 2021), together with regional and national soil datasets, were also used at several sites. For vegetation-derived carbon inputs, the Carnegie–Ames–Stanford Approach (CASA) model (Potter et al., 1993) was mainly employed to estimate aboveground biomass, which was subsequently used to calculate carbon inputs (see Appendix B.1 for details). Carbon inputs from organic amendments were mainly estimated from livestock numbers and manure production statistics (more details in Appendix B.2).

https://doi.org/10.5194/egusphere-2026-4735
Preprint. Discussion started: 9 September 2026

Table 2. Boundary conditions (BC) for all sites, including in-situ and remote sensing–derived data. (Data sources marked with * are described in detail in the Appendix B)

ID	BC1 Climate		BC2 Clay		BC3 initial SOC		BC4 Vegetation-derived Carbon inputs		BC5 Carbon inputs from organic amendments	
	In-situ	RS	In-situ	RS	In-situ	RS	In-situ	RS	In-situ	RS
DE-Crop-01	EC stations, climate in-situ dataset (Itzerott et al., 2018)	ERA5 dataset (Hersbach et al., 2020)	Soil sampling	Own Clay products from Airborne (HySpex, Brell et al., 2020) and satellite HRS data (PRISMA/EnMAP, Ward et al., 2024)	Soil sampling	Own SOC content products from Airborne (HySpex, Brell et al., 2020) and Satellite HRS data (PRISMA/EnMAP, Ward et al., 2024)	Calculated based on yield data, using Bolinder equation (Bolinder et al., 2007) to get C input.	Aboveground biomass (AGB) products from CASA model *[1]	Fertilization data from farm management	Not available
IT-Crop-02 & IT-Crop-03	Lamma network's meteorological station	ERA5 dataset	Soil sampling	Own clay model over the area through Random Forest + Sentinel data	Soil sampling	Own SOC model over the area through Random Forest + Sentinel-2 data	Calculated based on yield data and conversion factor to crop biomass.	AGB products from CASA model	No other carbon input, mineral fertilization only.	NA
CZ-Crop-04	EC stations, climate in-situ dataset	ERA5 dataset	Soil sampling, Proximal Sensing	Sentinel-2 & EnMAP data + Machine Learning approaches	Soil sampling, Proximal Sensing	Sentinel-2 & EnMAP data + Machine Learning approaches	Calculated based on yield data from farm management	AGB products from CASA model	Fertilization data from farm management	Based on statisticsc al livestocks numbers
BE-Crop-05	EC stations, climate in-situ dataset (Warm Winter 2020 Team & ICOS Ecosystem Thematic Centre, 2022)	TerraClimate dataset (Abatzoglou et al., 2018)	Soil sampling	Clay products of the Walloon Region (https://geoportail.wallonie.be/catalogue/e90eb7cf-8f7d-40ab-9df9-5c34ddf387ea.html)	Soil sampling	SOC products of the Walloon Region (Zhou et al., 2022)	Based on measured aboveground biomass values, using Bolinder equation (Bolinder et al., 2007) to get C input.	AGB products from CASA model	Fertilization data from farm management	Based on statisticsc al livestocks numbers*[2]
IT-Crop-06 & IT-Crop-07	Regional network weather station	ERA5 dataset	Soil sampling	Clay maps derived from CREA (https://zenodo.org/records/7746495)	Soil sampling	Own SOC model using Machine learning trained with ground truth data.	Yields derived from farmers interviews and local datasets. Biomass allocation coefficients and conversion factors to get C input.	AGB products from CASA model	Farm-level fertilisation record	NA
BE-Grass-01	EC stations, climate in-situ dataset (Warm Winter 2020 Team & ICOS Ecosystem Thematic Centre, 2022)	ERA5 Land dataset	Soil sampling	Clay products of the Walloon Region (https://geoportail.wallonie.be/catalogue/e90eb7cf-8f7d-40ab-9df9-5c34ddf387ea.html)	Soil sampling	SOC products of the Walloon Region (https://geoportail.wallonie.be/catalogue/47e4ea34-fe00-4712-b795-4a85fdab7dd7.html)	Based on measured aboveground biomass values, using formulas by C. Poeplau (2016) to get C input from aboveground and belowground biomass	AGB products from CASA model	Livestock number and grazing time from management data	Based on statisticsc al livestocks numbers*

https://doi.org/10.5194/egusphere-2026-4735
Preprint. Discussion started: 9 September 2026

SP-Grass-02	EC stations, climate in-situ dataset	ERA5 dataset	Soil sampling	SoilGrids (Poggio et al., 2021)	Soil sampling	SoilGrids (Poggio et al., 2021)	Calculated based on empirical formulas using NDVI > fPAR > APAR>NPP> fsoil (Field et al 1995; Bolinder et al. 2007; Geremew et al. 2024)	Calculated based on empirical formulas using NDVI > fPAR > APAR>NPP> fsoil (Field et al 1995; Bolinder et al. 2007; Geremew et al. 2024)	NA	NA
SP-Agrofor-01	CHELSA v2.1 dataset (Karger et al., 2017)	CHELSA v2.1 dataset	soil sampling - average clay data from the Level I plots of ICP-Forests Network	Clay product from Multi-temporal Earth Observation (EO) data from Sentinel-2 and Landsat missions (Palanza et al. 2026)	Soil sampling - average SOC stock from the Level I plots of ICP-Forests Network	SOC content product from Multi-temporal Earth Observation (EO) data from Sentinel-2 and Landsat missions (Palanza et al.2026). Bulk density from SoilGrids (Poggio et al., 2021)	C input from trees, shrubs and pasture using specific models (Ruiz-Peinado et al., 2011; Menéndez-Miguélez et al., 2022, Pasalodos-Tato et al., 2015, Torres et al., 2026)	Tree biomass products from CASA model	NA	NA
IT-Agrofor-02	Regional network weather station	In-situ historical timeseries+ERA5 dataset	Soil sampling	Clay maps derived from CREA (https://zenodo.org/records/7746495)	Soil sampling	Own SOC model using Machine learning trained with ground truth data.	Yield derived from local datasets and farmers interviews. Biomass allocation coefficients and conversion factors to get C input. Tree biomass calculated from DBH, height, and density. Allocation coefficients and IPCC/NIR conversion factors applied to quantify woody C input.	AGB products from CASA model	Farm-level fertilisation record	NA
CZ-Forest-01	EC stations, climate in-situ dataset	ERA5 dataset	Soil sampling, Proximal Sensing	SoilGrids (Poggio et al., 2021)	Soil sampling, Proximal Sensing	SoilGrids	Calculated from DBH, hight and tree density on site (Cerny et al., 1996)	Calculated based on growth tables and Czech allometric equations for biomass calculations (Pretzsch et al., 2014; Forrester et al., 2017)	NA	NA
SP-Forest-02	EC stations, climate in-situ dataset	ERA5 dataset	Soil sampling	SoilGrids (Poggio et al., 2021)	Soil sampling	SoilGrids (Poggio et al., 2021)	Calculated based on empirical	Calculated based on empirical	NA	NA

https://doi.org/10.5194/egusphere-2026-4735
Preprint. Discussion started: 9 September 2026

							formulas using NDVI > fPAR > APAR>NPP> fsoil (Field et al 1995; Bolinder et al. 2007; Geremew et al. 2024)	formulas using NDVI > fPAR > APAR>NPP> fsoil (Field et al 1995; Bolinder et al. 2007; Geremew et al. 2024)		
IT-ForPlan-01 & IT-ForPlan-02	In-situ meteorological station	In-situ historical timeseries+ERA5 dataset	Soil sampling	Clay maps derived from CREA (https://zenodo.org/records/7746495)	Soil sampling	Own SOC model using Machine learning trained with ground truth data.	Tree biomass calculated from DBH, height, and density. Allocation coefficients and IPCC/NIR conversion factors applied to quantify woody C input.	AGB products from CASA model	NA	NA
SP-shrub-01	EC stations, climate in-situ dataset	ERA5 dataset	Soil sampling	SoilGrids (Poggio et al., 2021)	Soil sampling	SoilGrids (Poggio et al., 2021)	Calculated based on empirical formulas using NDVI > fPAR > APAR>NPP> fsoil (Field et al 1995; Bolinder et al. 2007; Geremew et al. 2024)	Calculated based on empirical formulas using NDVI > fPAR > APAR>NPP> fsoil (Field et al 1995; Bolinder et al. 2007; Geremew et al. 2024)	NA	NA

https://doi.org/10.5194/egusphere-2026-4735
Preprint. Discussion started: 9 September 2026

2.2 Simulation design

We developed and applied a general framework to quantify boundary-condition sensitivity in SOC modelling (Table 3). Key boundary conditions required for regional-scale SOC modelling, including climate variables, soil texture, initial SOC stocks, vegetation-derived carbon inputs, and management-related organic amendments (e.g. farmyard manure), are listed in Table 2. A reference baseline simulation (S00_in_situ) was first established using boundary conditions derived entirely from in-situ observations or site-specific measurements. These simulations are treated as internally consistent reference trajectories and are not assumed to represent ground truth SOC dynamics. To isolate the sensitivity of SOC simulations to individual boundary conditions, we adopted a one-at-a-time substitution strategy. Starting from the in-situ baseline simulation, each boundary condition was replaced individually by its remote sensing–derived alternative, while all other inputs were held constant (S01-05). In addition, a scenario was implemented in which all boundary conditions were replaced simultaneously using remote sensing–based datasets (S06_RS).

All subsequent analyses compared simulations driven by boundary-condition substitution simulations (S01–06) against the in-situ baseline simulation (S00_in_situ).

Table 3. Summary of the simulations under different input data combinations (Cells in regular font represent in-situ data; cells in bold font represent remote-sensing or agricultural census data.)

S00_in_situ	Climate	Clay	Initial SOC	Cinput_veg	Cinput_org
S01_Climate	**Climate**	Clay	Initial SOC	Cinput_veg	Cinput_org
S02_Clay	Climate	**Clay**	Initial SOC	Cinput_veg	Cinput_org
S03_Initial_SOC	Climate	Clay	**Initial SOC**	Cinput_veg	Cinput_org
S04_Cinput_veg	Climate	Clay	Initial SOC	**Cinput_veg**	Cinput_org
S05_Cinput_org	Climate	Clay	Initial SOC	Cinput_veg	**Cinput_org**
S06_RS	**Climate**	**Clay**	**Initial SOC**	**Cinput_veg**	**Cinput_org**

*Cinput_veg: vegetation-derived carbon inputs; Cinput_org: carbon inputs from organic amendments

Given the diversity of sites and data availability, individual sites were allowed to initialize and run the model using configurations considered most appropriate for their respective conditions. As a result, modelling protocols may differ slightly among sites, although all simulations follow the same general modelling framework (Table 3) and input structure. In particular, model initialization procedures, which ensure that the model starts from a steady-state equilibrium, varied depending on data availability. For sites with multiple SOC observations, spin-up was performed under long-term average conditions by iteratively adjusting carbon inputs until the modelled SOC matched observed initial SOC stocks. This approach ensures consistency between model initialization and measured SOC conditions. For sites with only a single SOC observation, a long-term spin-up (e.g. 1000 years) was conducted under constant input conditions until SOC reached equilibrium prior to the start of simulations. In addition, not all substitution scenarios were applicable to all sites. For example, the substitution of organic amendments (*S05_Cinput_org*) was only conducted for cropland sites.

https://doi.org/10.5194/egusphere-2026-4735
Preprint. Discussion started: 9 September 2026

2.3 Sensitivity Quantification

In this study, boundary-condition sensitivity evaluates how SOC simulations respond to the substitution of in situ boundary conditions by remote sensing–derived datasets. To qualify boundary-condition sensitivity, the in-situ baseline simulation (*S00_in_situ*) was compared with boundary-condition substitution simulations (*S01–06*). Unlike classical model accuracy or uncertainty assessments, which evaluate agreement between simulations and observations, the present analysis focused on differences between baseline and substitution simulations.

Sensitivity was evaluated from two complementary perspectives:

(1) Dynamic sensitivity: assess changes in the temporal trajectories of simulated SOC stocks between baseline and substitution simulations by comparing the complete SOC time series. Dynamic sensitivity was quantified using R^2, nRMSE, and the decomposition components of RMSE (see sections below for detailed description).

(2) Endpoint sensitivity: assess whether the same substitutions affected estimated SOC stock changes over defined reporting periods by comparing SOC differences (ΔSOC) between the beginning and end of the simulation period. Endpoint sensitivity was quantified using differences in ΔSOC over fixed and rolling time windows.

Five typical pattern types between baseline and substitution simulation are summarized in Fig. 1, including complete consistency, pure offset, noise-like variation, slope mismatch, and inconsistency. These examples illustrate different combinations of trajectory and endpoint behaviours, and their corresponding expected responses in dynamic and endpoint sensitivity metrics. However, actual simulation differences are often more complex and may represent combinations of multiple pattern types.

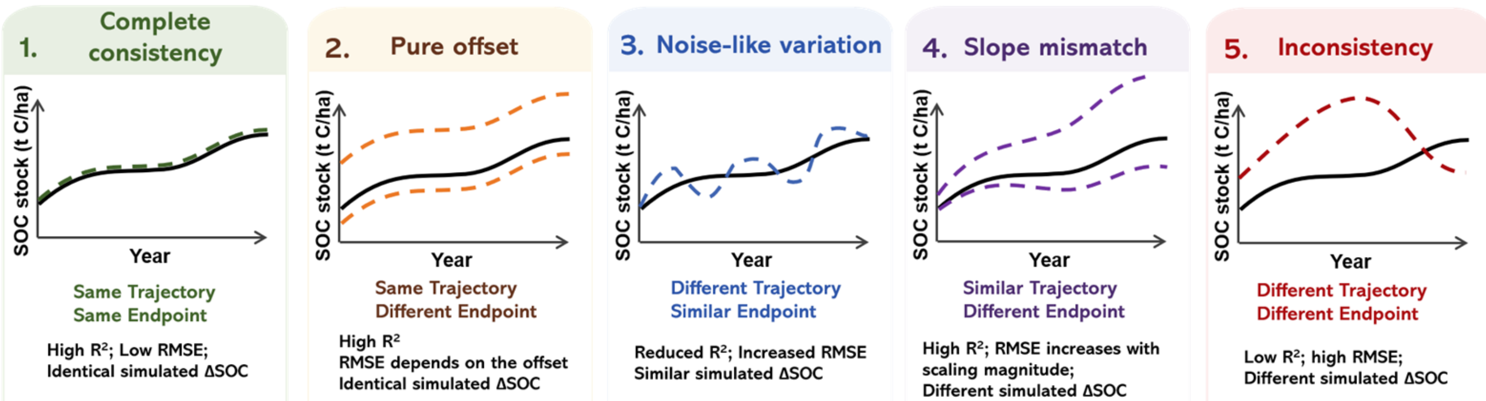

Figure 1: Five typical pattern types between in-situ baseline simulation (S00_ in situ; black solid line) and substitution simulations (S01-S06; coloured dashed line).

To support the understanding of the calculations, a site-specific simulation example is presented in Fig. 2, where the baseline simulation is denoted as X and the substitution simulation as Y. SOC outputs were available at n discrete time steps over the full simulation period, defined as the longest temporal extent allowed by site-specific data availability. All equations and calculations presented in the following subsections are based on this framework.

https://doi.org/10.5194/egusphere-2026-4735
Preprint. Discussion started: 9 September 2026

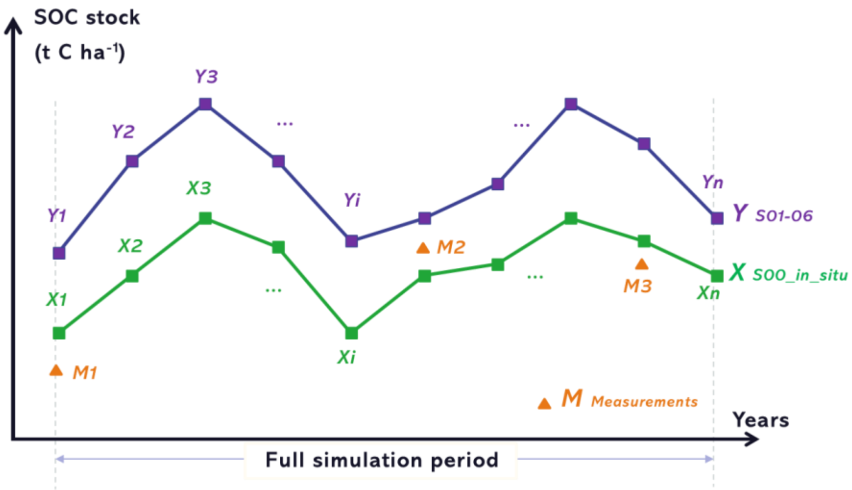

Figure 2: Comparison of SOC time series between baseline and substitution simulation.

Despite this study focusing on boundary-condition sensitivity rather than model accuracy, a reliable baseline simulation is essential to ensure meaningful sensitivity analysis. Therefore, classical model evaluation metrics ($RMSE_{model\text{-}obs}$ and $R^2_{model\text{-}obs}$; see Section 2.3.1 for definitions) were separately calculated for (i) observed and simulated final SOC stocks (M vs. X in Fig. 2) and (ii) observed and simulated SOC changes over the simulation period (ΔM vs. ΔX) to evaluate the reliability of the baseline simulations. Unlike their application in Section 2.3.1, where RMSE and R^2 quantify deviations between baseline and substitution simulations, here the same metrics assess the agreement between simulated and observed SOC stocks and SOC changes.

2.3.1 General dynamic sensitivity

Dynamic sensitivity was first quantified by comparing the entire SOC time-series trajectories obtained from each boundary-condition substitution (Y; *S01–06*) with the corresponding in situ baseline simulation (X; S00_in_situ). The coefficient of determination (R^2, Eq. 1) was calculated as the squared Pearson correlation coefficient between the baseline simulation (X) and the substitution simulation (Y), representing the degree of temporal coherence between two time series. The root mean squared error (RMSE, Eq. 2) was normalised by the mean SOC stock of the baseline simulation to obtain the normalised root mean squared error (nRMSE, Eq. 3), enabling comparisons across sites with different SOC levels and quantifying the overall magnitude of deviations. These metrics were further grouped by land-use type, and the mean and standard deviation were calculated to assess differences in boundary-condition sensitivity among land-use categories.

$$R^2 = r^2 = \frac{\left(\sum_{i=1}^{n}(X_i - \bar{X})(Y_i - \bar{Y})\right)^2}{\left(\sum_{i=1}^{n}(X_i - \bar{X})^2\right)\left(\sum_{i=1}^{n}(Y_i - \bar{Y})^2\right)} \tag{1}$$

$$RMSE = \sqrt{\frac{1}{n}\sum_{i=1}^{n}(Y_i - X_i)^2} \tag{2}$$

https://doi.org/10.5194/egusphere-2026-4735
Preprint. Discussion started: 9 September 2026

$$nRMSE = \frac{RMSE}{\bar{X}} \quad (3)$$

where X_i and Y_i represent SOC values from the baseline and substitution simulations at time step i, respectively (Fig. 2). The index i runs over all time steps of the full simulation period (e.g. monthly or yearly outputs), and n is the total number of time steps. $\bar{X}$ and $\bar{Y}$ are the means of X and Y, respectively.

2.3.2 Decomposition of mean squared deviation

To further characterise the structure of dynamic sensitivity and distinguish different types of sensitivity in temporal SOC dynamics, we decomposed the mean squared deviation (MSD) between the baseline simulation (*S00_in_situ*) and the boundary-condition substitution simulations (*Simulations 01–06*) following the approach of Gauch et al. (2003). This decomposition allows the total deviation between two time series to be partitioned into additive and non-overlapping components associated with distinct error structures. The MSD was calculated as the squared value of RMSE (Eq. 4) and further decomposed into three components (Eq. 5): squared bias (SB), the non-unity slope component (NU), and the lack-of-correlation component (LC).

$$MSD = RMSE^2 \quad (4)$$

$$MSD = SB + NU + LC \quad (5)$$

The SB component represents systematic offset in the mean SOC level between simulations and is defined as Eq. 6.

$$SB = (\bar{Y} - \bar{X})^2 \quad (6)$$

where $\bar{X}$and $\bar{Y}$ are the means of X_i and Y_i, respectively.

The NU component quantifies differences in the strength of SOC temporal dynamics between simulations and is expressed as Eq. 7.

$$NU = (1 - b)^2 \times \frac{\sum_{i=1}^{n}(X_i - \bar{X})^2}{n} \quad (7)$$

where b is the slope of the ordinary least-squares regression of Y on X (Eq.8).

$$b = \frac{\sum_{i=1}^{n}(X_i - \bar{X})(Y_i - \bar{Y})}{\sum_{i=1}^{n}(X_i - \bar{X})^2} \quad (8)$$

The LC component represents deviations associated with reduced temporal coherence between simulations, reflecting mismatches in temporal patterns not explained by systematic bias or differences in dynamic strength, and is given by Eq. 9.

$$LC = (1 - r^2) \times \frac{\sum_{i=1}^{n}(Y_i - \bar{Y})^2}{n} \quad (9)$$

where $r^2$is the squared Pearson correlation coefficient between X and Y, equivalent to the R^2 term in Eq. 1.

The characteristic deviations represented by these three components correspond to the "Pure offset (SB)", "Slope mismatch (NU)" and "Noise-like variation (LC)" patterns shown in Fig. 1.

https://doi.org/10.5194/egusphere-2026-4735
Preprint. Discussion started: 9 September 2026

As absolute MSD values varied substantially across sites, the contributions of SB, NU, and LC were further normalised by the total MSD and expressed as relative proportions. This normalisation facilitates comparison among sites and enables a clearer interpretation of the dominant sources of sensitivity in SOC temporal dynamics.

2.3.3 Endpoint sensitivity

Since SOC stock changes are often reported using endpoint differences, we explicitly quantify how substituting in situ boundary conditions with RS-derived inputs affects endpoint SOC stock change. Here, we propose two approaches for evaluating endpoint sensitivity to boundary-condition substitution.

Fixed endpoint sensitivity (Fixed ES). For each site, the full simulation period was used, and SOC change (ΔSOC) was calculated as the difference between SOC stocks at the first and last simulation years. Fixed endpoint sensitivity was then quantified as the difference in ΔSOC between each boundary-condition substitution simulation (*Simulations 01–06*) and the in-situ baseline simulation (*S00_in_situ*) over the same period as Eq.10.

$$Fixed\ ES\ = \Delta SOC_Y - \Delta SOC_X = \left(\bar{Y}_m - \bar{Y}_1\right) - \left(\bar{X}_m - \bar{X}_1\right) \tag{10}$$

where $\bar{X}_1$ and $\bar{X}_m$ denote the average SOC stocks in the first and last simulation years of the baseline simulation, respectively, whereas $\bar{Y}_1$ and $\bar{Y}_m$ represent the corresponding values from the substitution simulations. If SOC outputs were available on a yearly basis, these values were used directly; otherwise, for simulations with monthly outputs, SOC values of endpoint years were first aggregated into annual means before calculating ΔSOC.

To enable easier comparison across simulations with different simulation periods and initial SOC levels, we further calculated annualized and normalized Fixed ES (Eq. 11 & 12):

$$Annualized\ Fixed\ ES\ = \frac{Fixed\ ES}{(m-1)} \tag{11}$$

$$Normalized\ Fixed\ ES\ = \frac{Fixed\ ES}{(m-1) \times \bar{X}_1} \tag{12}$$

where $(m-1)$ is the total number of simulation years, given m is the last simulation year.

Rolling window endpoint sensitivity (Rolling window ES). To assess whether endpoint sensitivity depends on the length of the reporting period, we applied a rolling time window approach. For each site, analyses started with the shortest reporting window of three years and progressively extended the window length over the full simulation period.

For each time window, SOC change (ΔSOC) was calculated as the difference between SOC stocks at the start and end years of the window for both the baseline and substitution simulations, and the rolling window endpoint sensitivity was then defined as Eq. 13.

$$\begin{aligned} Rolling\ window\ ES\ (t,k) &= \Delta SOC_Y(t,k) - \Delta SOC_X(t,k) \\ &= (\bar{Y}_{t+k} - \bar{Y}_t) - (\bar{X}_{t+k} - \bar{X}_t) \end{aligned} \tag{13}$$

https://doi.org/10.5194/egusphere-2026-4735
Preprint. Discussion started: 9 September 2026

where k is the length of the reporting window (in years) and t is the starting year of the window. For a simulation with $(m - 1)$ years ($m \geq 3$), k ranges from 3 to $(m-1)$, and t ranges from 1 to $m-k$. $\bar{X}$ and $\bar{Y}$ are the average SOC stocks for a given year from the baseline and substitution simulations, respectively.

For a given window length k, the rolling window endpoint sensitivity was calculated as the mean of all $ES(t,k)$ values. For example, for a 3-year window with yearly outputs, SOC changes for the baseline simulation were calculated as $\bar{X}_4 - \bar{X}_1$, $\bar{X}_5 - \bar{X}_2$, …, $\bar{X}_m - \bar{X}_{m-3}$. The corresponding endpoint sensitivity for the 3-year window was then obtained by averaging all $ES(t,3)$ values.

Coherence of SOC change direction. In addition to absolute differences, we evaluated the consistency in the direction of SOC change between simulations, as this determines whether a system is classified as a carbon sink or a carbon source. For each window length k, the signs of all $\Delta SOC_X(t,k)$ and $\Delta SOC_Y(t,k)$ values were compared across the corresponding starting times t, resulting in four possible combinations: (++), (−−), (+−), and (−+), where + indicates an increase in SOC and − indicates a decrease. The first sign refers to the baseline simulation (*S00_in_situ*), and the second to the substitution simulation. The first two combinations indicate directional agreement, whereas the latter two indicate directional disagreement. For each window length k, the frequency of these four sign combinations was calculated across all valid t, and the most frequently occurring combination was taken as the coherence result for that window length.

3 Results

3.1 baseline simulation performance

Figure 3 compares the final observed SOC stocks with the corresponding predictions from the baseline simulation (*S00_in situ*) (Fig. 3A). Overall, the baseline simulation showed good agreement with the observations across all study sites, with an $R^2_{model\text{-}obs}$ of 0.85. This supports the use of *S00_in_situ* as a consistent and reliable reference for subsequent sensitivity analyses. In addition, the observed and simulated SOC stock changes (ΔSOC) between the first and final observation periods was compared for sites with at least two SOC sampling events (Fig. 3B). The baseline simulation also reproduced SOC stock changes with good accuracy ($R^2_{model\text{-}obs} = 0.80$), and 79% of the sites showed consistent directions of SOC change between the simulations and observations.

https://doi.org/10.5194/egusphere-2026-4735
Preprint. Discussion started: 9 September 2026

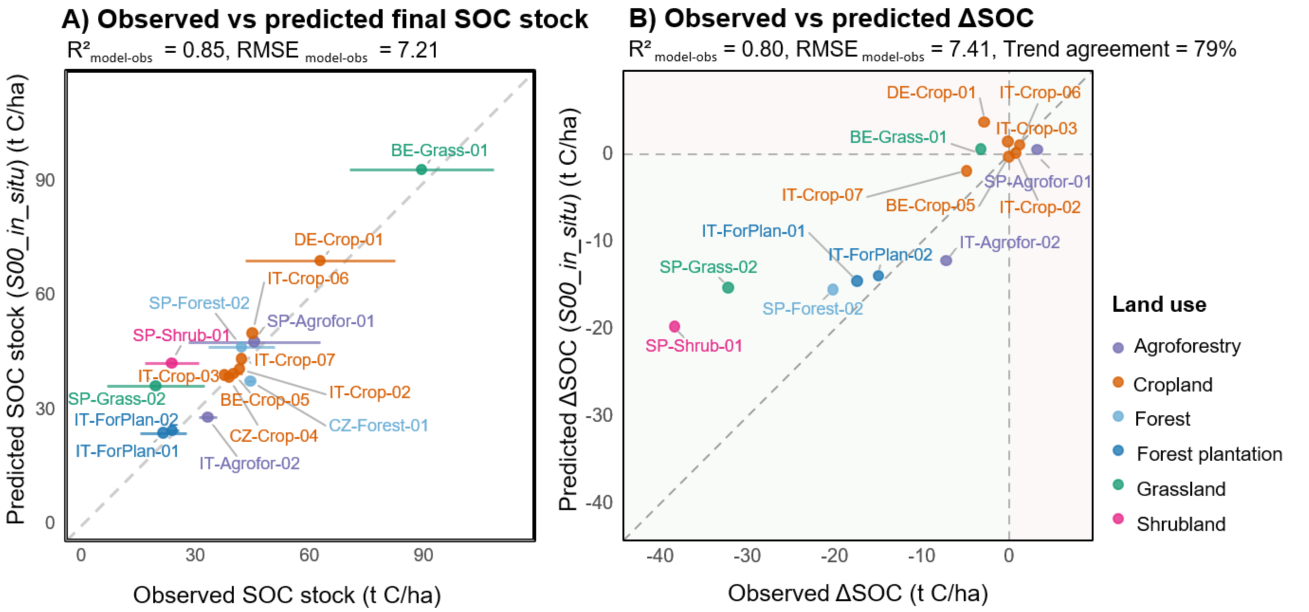

Figure 3: Performance of the baseline simulation (S00_in situ). (A) Comparison between observed and simulated final SOC stocks. (B) Comparison between observed and simulated SOC stock changes (ΔSOC) between the first and final observation periods. Green areas indicate agreement in the direction of SOC change between observations and simulations, whereas red areas indicate disagreement.

3.2 General dynamic sensitivity to boundary-condition substitution

3.2.1 Overall dynamic sensitivity across sites

General dynamic sensitivity varied substantially across all site–simulation combinations (Fig. 4), with nRMSE values ranging from 0 to 0.68 and R^2 values spanning nearly the full theoretical range (0.0001–1).

Across boundary-condition substitutions, replacing the initial SOC stock with remote sensing–derived inputs introduced the largest dynamic sensitivity, with nRMSE values exceeding 0.4 at several sites, particularly SP-Grass-02, SP-Forest-02, and SP-Shrub-01. This effect was not consistent across all sites. At CZ-Crop-04, BE-Crop-05, IT-Crop-07, and CZ-Forest-01, substituting the initial SOC stock resulted in negligible dynamic sensitivity, with nRMSE values close to zero. High nRMSE values observed in the *S03_Initial_SOC* scenario were also reflected in the fully substituted scenario (*S06_RS*), leading to similarly large deviations at these Spanish sites. In contrast, replacing climate and clay content (*S01_Climate & S02_Clay*) introduced relatively low nRMSE across most sites.

A notable contrast was observed in the relationship between nRMSE and R^2. At the Spanish sites where replacing the initial SOC stock resulted in high nRMSE values, replacing the initial SOC stock also led to R^2 values close to unity, indicating large absolute deviations despite strong temporal agreement.

https://doi.org/10.5194/egusphere-2026-4735
Preprint. Discussion started: 9 September 2026

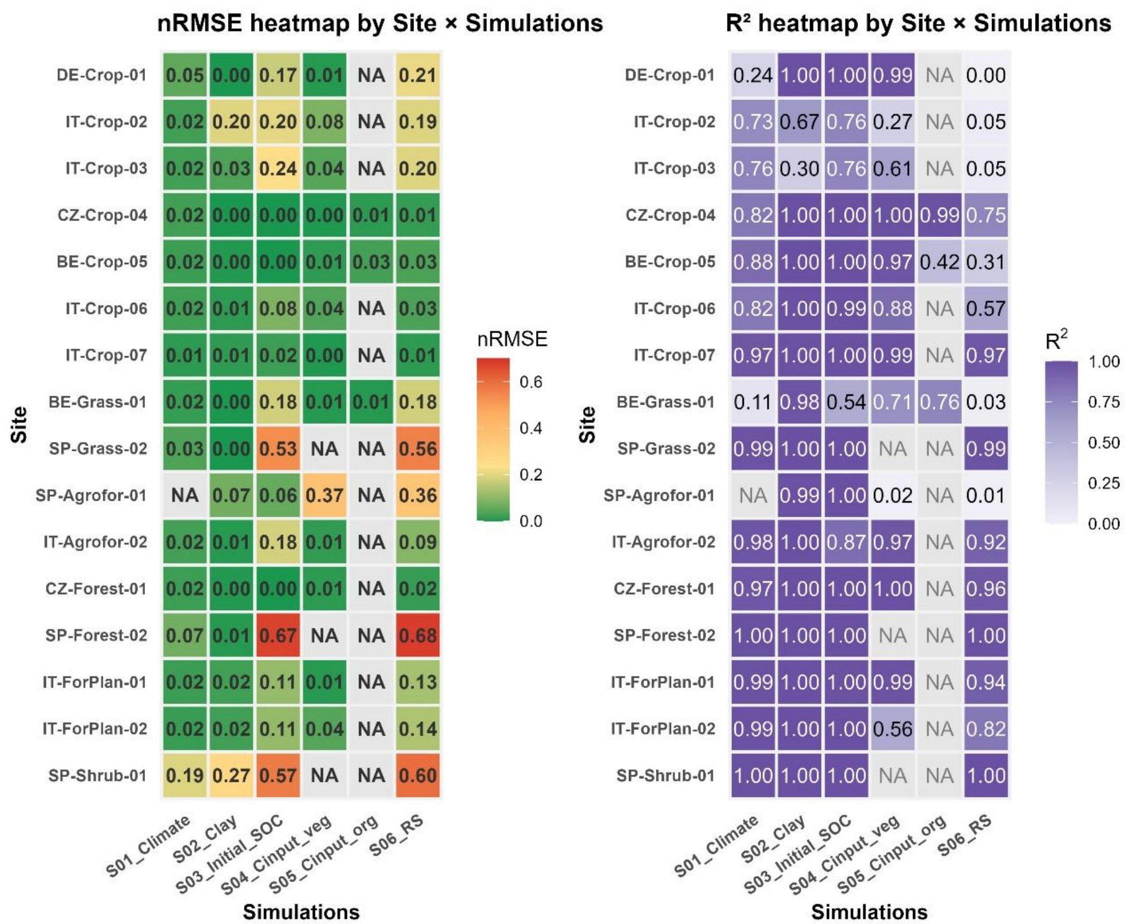

Figure 4: Heatmaps of dynamic sensitivity metrics (nRMSE and R^2) across sites and simulations (S01–06 vs S00_in_situ).

3.2.2 Dynamic sensitivity stratified by land-use type

Mean nRMSE values varied across land-use categories (Fig. 5). Substitutions of climate (*S01_Climate*) and carbon inputs from organic amendments (*S05_Cinput_org*) resulted in low mean nRMSE values across all simulations. When replacing the initial SOC stock (*S03_Initial_SOC*) or soil clay content (*S02_Clay*), cropland sites exhibited lower nRMSE values compared to other land-use types (grassland, forest, and shrubland). This lower dynamic sensitivity (nRMSE) in cropland sites is consistent with generally lower RMSE reported for cropland soil property estimates in previous prediction studies (Zhou et al., 2022; Stumpf et al., 2024). Relatively high nRMSE values were observed for vegetation-derived C input substitution (*S04_Cinput_veg*) in the agroforestry category, mainly driven by SP-Agrofor-01.

https://doi.org/10.5194/egusphere-2026-4735
Preprint. Discussion started: 9 September 2026

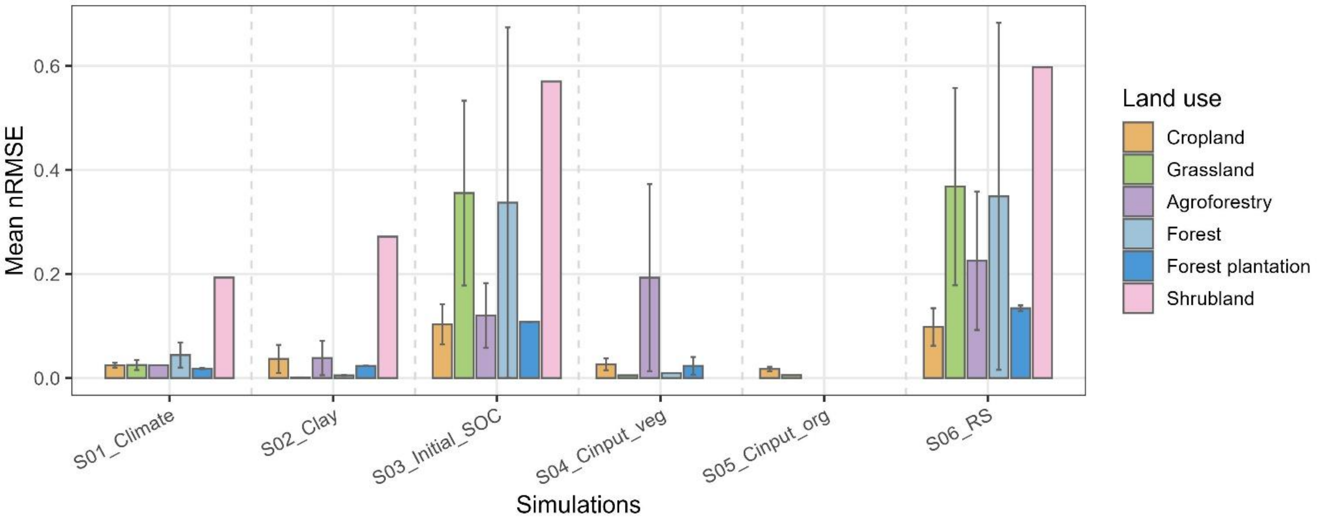

Figure 5: Mean nRMSE across land-use types for different boundary-condition substitution simulations. Error bars represent standard deviation across sites.

3.3 Decomposition of dynamic sensitivity

MSD was decomposed into its three components (SB, NU, and LC), and the relative contribution of each component was calculated (Fig. 6). The decomposition clearly shows that substituting different boundary conditions leads to distinct MSD structures across sites. For substitutions related to climate, clay content, and vegetation-derived carbon inputs, no consistent MSD pattern emerged, with the relative contributions of SB (squared bias), NU (non-unity), and LC (lack-of-correlation) varying among sites.

In contrast, substitution of the initial SOC stock exhibited a highly consistent MSD structure across sites, with the total MSD almost entirely dominated by the SB component. This indicates that differences arising from initial SOC substitution primarily reflect systematic offsets in SOC levels, while temporal trajectories remain similar. When *S00_in_situ* and *S03_Initial_SOC* were compared (Fig. A.1), the simulations differed mainly in their start point (initial SOC stocks) but followed nearly identical temporal path.

A distinct site-specific pattern was observed for the substitution of organic amendments at site BE-Crop-05. In this case, MSD was almost entirely dominated by the LC and NU components, indicating reduced temporal coherence and changes in trajectory slope between the baseline simulation (*S00_in_situ*) and the substitution simulation (*S05_Cinput_org*). Site-specific management records indicate that organic amendments are applied approximately every five years at this site, whereas in the simulations organic amendments were added annually based on livestock numbers and manure production. This mismatch in the timing of carbon inputs resulted in misaligned SOC trajectories, leading to increased contributions from LC and NU (Fig. A.2). Although alternative assumptions (e.g. manure application every three or five years) could also be adopted, such assumptions would not be universally applicable across all sites because field-level application frequency is generally unavailable in large-scale datasets. Consequently, any generalized assumption regarding application timing would inevitably introduce temporal mismatches in carbon inputs, leading to similar MSD decomposition patterns.

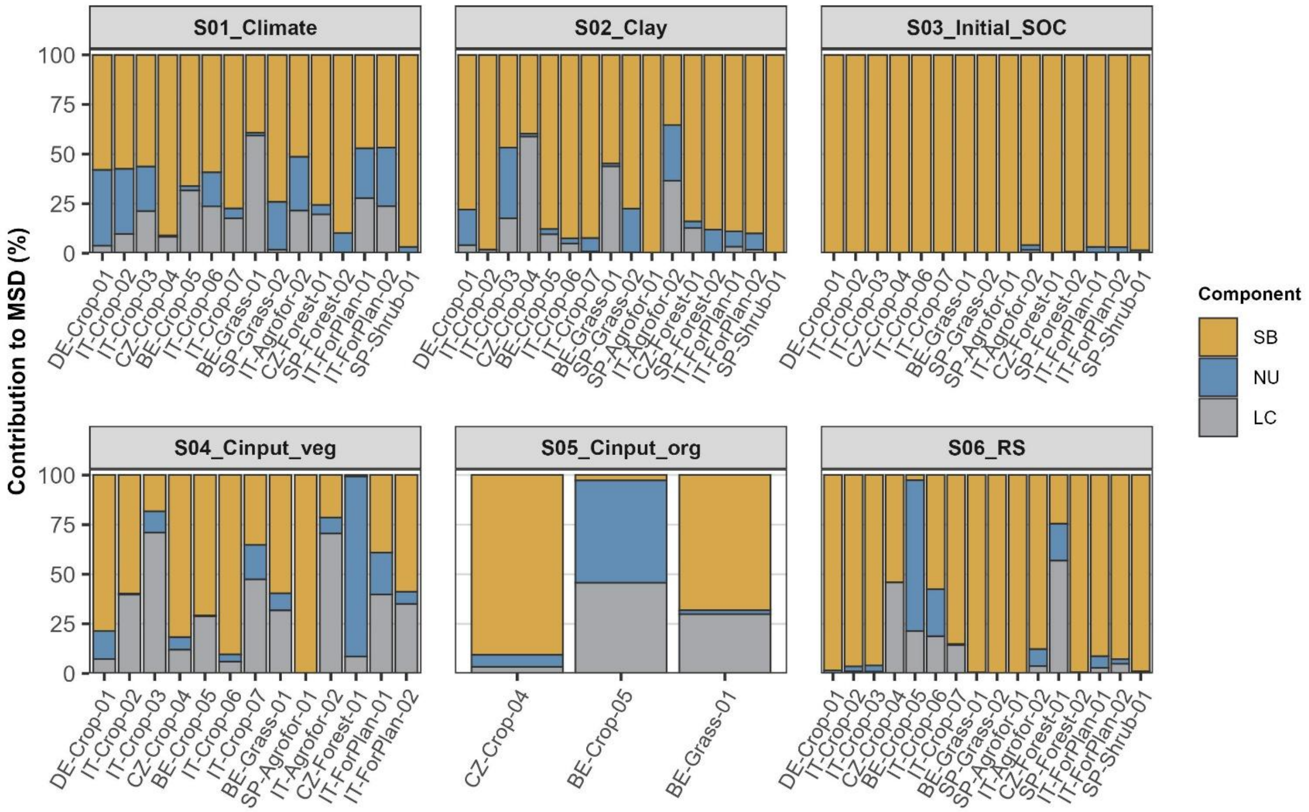

Figure 6: Mean squared deviation (MSD) decomposition for different simulations across all sites. (SB: squared bias; NU: non-unity slope; LC: lack-of-correlation).

3.4 Endpoint Sensitivity results

3.4.1 Fixed endpoint sensitivity

Annualized and normalized fixed-endpoint sensitivity across all sites and simulations is shown in Fig. 7. First, endpoint sensitivity differed among boundary-condition substitutions. Substitution of climate inputs (*S01_Climate*) resulted predominantly in negative endpoint sensitivities, indicating that replacing in situ climate data with RS-derived inputs generally led to lower estimated SOC changes relative to the baseline simulation. In contrast, substitution of the initial SOC stock (*S03_Initial_SOC*) more frequently produced positive endpoint sensitivities.

For *S06_RS*, most sites exhibited relatively small annualized endpoint sensitivity, with absolute values below 0.16 t C ha^{-1} yr^{-1}. In contrast, DE-Crop-01 and IT-Crop-06 showed relatively large negative sensitivity, whereas BE-Grass-01, SP-Grass-02, SP-Forest-02, and SP-Shrub-01 exhibited relatively large positive sensitivity. Normalized endpoint sensitivity showed a similar pattern. However, the two forest plantation sites exhibited comparatively higher normalized sensitivity because of their

https://doi.org/10.5194/egusphere-2026-4735
Preprint. Discussion started: 9 September 2026

relatively low average SOC stocks, corresponding to annual sensitivity deviations of approximately 0.5% of their SOC stock level.

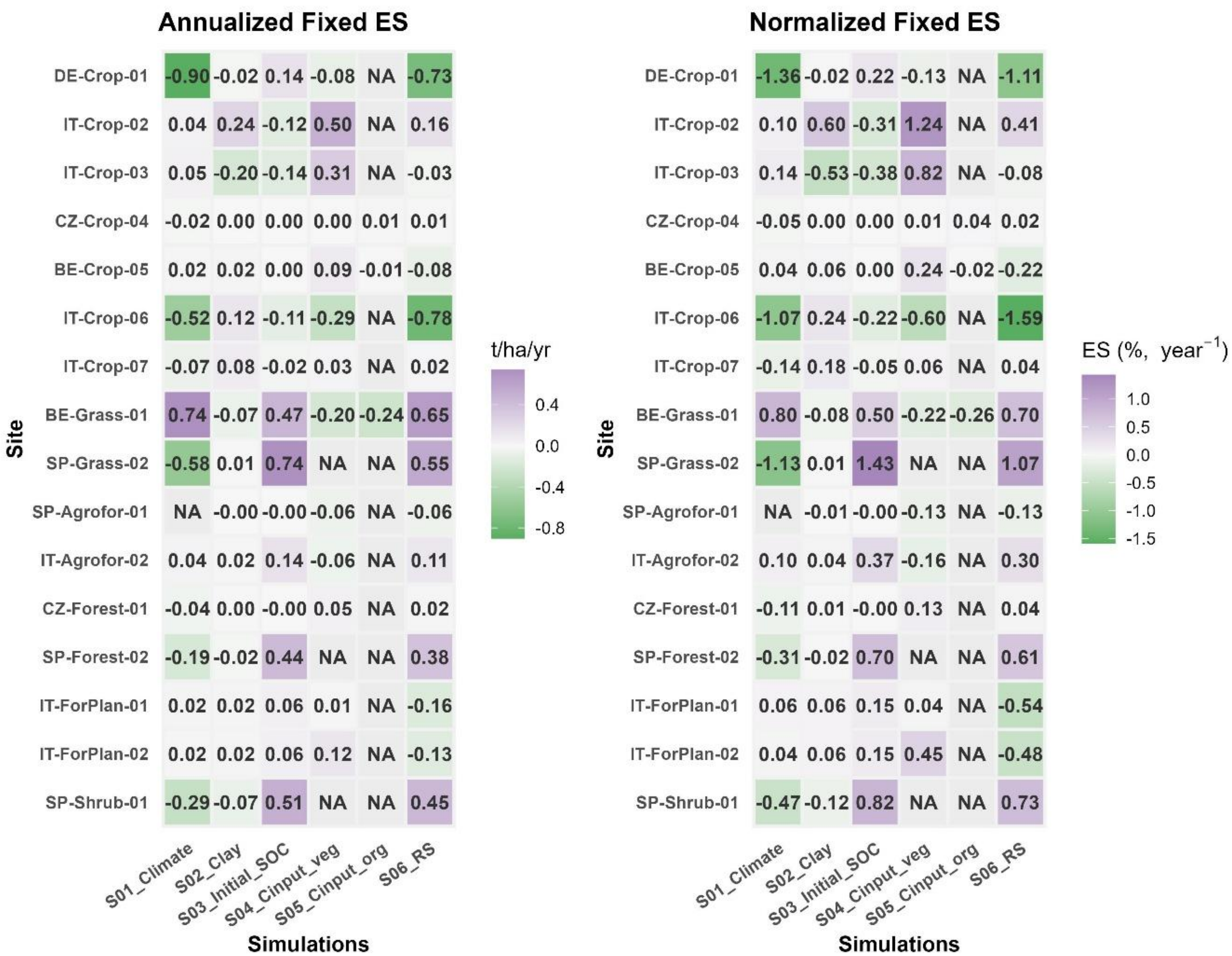

Fig 7: (left, t C ha^{-1} yr^{-1}) and normalized (right, % yr^{-1}) fixed endpoint sensitivity (ES) across all sites and boundary-condition substitution scenarios.

3.4.2 Rolling endpoint sensitivity

The rolling endpoint sensitivity results for the fully remote-sensing–driven simulation (*S06_RS*) are shown in Fig. 8. Across all sites, the magnitude of the average endpoint sensitivity increased with the length of the reporting window. Both positive and negative endpoint differences tended to deviate further from zero, indicating that longer simulation periods led to larger deviations from the baseline when absolute SOC stock changes were considered.

https://doi.org/10.5194/egusphere-2026-4735
Preprint. Discussion started: 9 September 2026

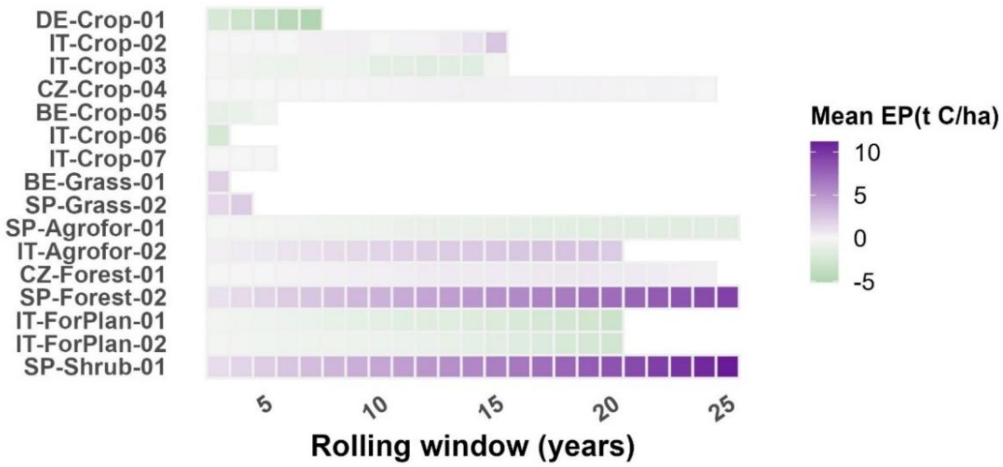

Figure 8: Rolling Endpoint Sensitivity (EP) Heatmap comparing S00_in_situ and S06_RS.

We further examined whether the direction of simulated SOC change (sink vs. source) under different reporting windows was consistent with that of the baseline simulation (Fig. 9). Focusing on *S06_RS*, almost all sites eventually reproduced the same direction of SOC change as the baseline.

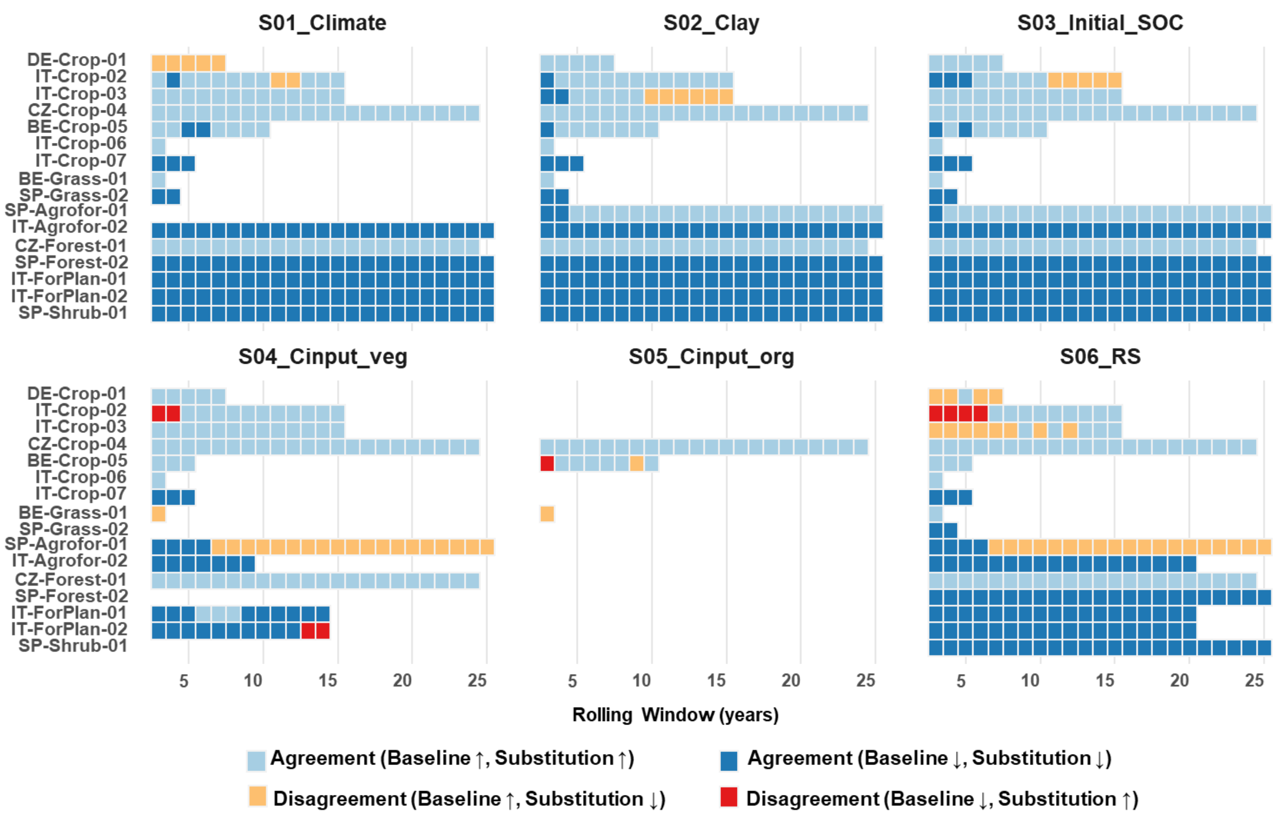

Figure 9: Heatmap of SOC change direction agreement across sites and simulations.

https://doi.org/10.5194/egusphere-2026-4735
Preprint. Discussion started: 9 September 2026

At IT-Crop-02 and IT-Crop-03, the simulations initially predicted incorrect SOC change directions, with one case misclassifying a carbon source as a sink and the other showing the opposite. However, after around 10-15 years, the simulated directions converged to those of the baseline. At site DE-Crop-01, the simulation mostly predicted a carbon source, whereas the baseline indicated a carbon sink. Examination of other subplots suggests that this discrepancy is primarily driven by the substitution of climate inputs (*S01_Climate*). Similarly, SP-Agrofor-01 misclassified a carbon sink as a carbon source, mainly associated with the substitution of vegetation-derived C inputs (S04_Cinput_veg).

4 Discussion

4.1 Dynamic and endpoint sensitivity capture different dimensions of model performance

Replacing in-situ boundary conditions with remote sensing–derived data is not a neutral substitution in SOC modelling. Boundary-condition substitution can alter both the temporal trajectory of SOC dynamics and the endpoint estimates used for carbon accounting. To capture these different effects, we distinguish between dynamic sensitivity, which characterizes changes in temporal SOC trajectories, and endpoint sensitivity, which quantifies deviations in reported SOC change over defined reporting periods.

Unlike conventional model evaluation, which compares simulations against observations using metrics such as R^2 and nRMSE (Studdert et al., 2011; Wang et al., 2026), our framework isolates the influence of boundary-condition substitution by comparing baseline simulations with substitution simulations. Within this context, nRMSE reflects the magnitude of deviations introduced by input substitution, whereas R^2 characterizes the temporal coherence between baseline and substitution simulations. Consequently, simulations may exhibit high R^2 despite large nRMSE values (Fig. 4), indicating that temporal coherence can be maintained even when substantial systematic offsets exist. This highlights that dynamic sensitivity cannot be adequately characterized by a single metric.

Dynamic and endpoint sensitivity also provide complementary rather than interchangeable information. For example, MSD decomposition indicates that some fully substituted simulations (e.g. *S06_RS* of SP-Forest-02 and SP-Shrub-01; Fig. 6) are dominated by the SB component, suggesting that deviations are primarily systematic offsets. However, rolling endpoint sensitivity continued to increase with reporting window length (Fig. 8), indicating that endpoint divergence accumulated over time despite the apparent dominance of SB. This apparent inconsistency arises because dynamic sensitivity describes deviations at individual time steps, whereas endpoint sensitivity reflects their cumulative effects over time. Consequently, although the dominant SB component can mask the smaller contributions of NU and LC, their cumulative effects become increasingly apparent in long-term endpoint estimates.

These findings demonstrate that dynamic and endpoint sensitivity address different modelling questions and should therefore be interpreted according to the intended application. Dynamic sensitivity is more informative when evaluating SOC dynamics or temporal responses, whereas endpoint sensitivity is more relevant for applications based on endpoint SOC estimates, including carbon accounting, target-year reporting, and sink/source classification. Together, they provide a more

https://doi.org/10.5194/egusphere-2026-4735
Preprint. Discussion started: 9 September 2026

comprehensive basis for evaluating the robustness of SOC simulations under boundary-condition substitution than either perspective alone.

4.2 Understanding the magnitude and structure of dynamic sensitivity in SOC modelling

4.2.1 Magnitude of sensitivity and priorities for improving data input quality

The magnitude of boundary-condition sensitivity varies across different substitutions and evaluation metrics. Despite heterogeneity across sites in modelling approaches, input datasets, land use types, and simulation periods, several consistent patterns emerge across sites. Among all boundary conditions, initial SOC stocks, vegetation-derived carbon inputs and climate data are identified as dominant sources of sensitivity. Substituting initial SOC typically results in large deviations in SOC levels, reflected by high nRMSE values, while replacing vegetation-derived carbon inputs and climate data tends to reduce temporal coherence, as indicated by lower R^2. In contrast, currently available soil clay datasets introduce relatively limited sensitivity, suggesting that they are relatively robust for large-scale SOC modelling applications. These results indicate that efforts to improve SOC modelling performance should not be uniformly distributed across all inputs, but rather prioritised towards boundary conditions that exert the strongest influence on model sensitivity.

For the substitution of initial SOC, digital soil mapping (DSM; McBratney et al., 2003) is the dominant approach for generating spatially explicit SOC maps by integrating field observations, environmental covariates, and remote sensing products (Arrouays et al., 2020; Chen et al., 2022). However, its predictive accuracy remains spatially heterogeneous and is strongly influenced by sampling density and landscape complexity (Lagacherie et al., 2020; Liu et al., 2022). This is reflected in our results, where sensitivity to initial SOC varies substantially across land-use types (e.g. nRMSE in Fig. 5). Cropland and agroforestry systems generally show lower sensitivity, whereas grassland and forest sites exhibit much larger deviations when initial SOC is substituted.

This difference can be attributed not only to better data availability of management (Zhou et al., 2022) and more intensive soil monitoring in croplands (Stumpf et al., 2024), but also to differences in the approaches used to derive spatial SOC information. Periodic bare-soil conditions (Safanelli et al., 2020) allow multispectral and hyperspectral remote sensing to directly retrieve soil properties with higher accuracy, whereas persistent vegetation cover in grasslands and forests limits direct soil observation and increases reliance on DSM approaches, resulting in greater prediction uncertainty. Improving SOC map quality in these systems therefore requires increased observations and modelling approaches that better account for complex land-cover conditions (Lagacherie et al., 2020; Huang et al., 2022). Future improvements are also expected from new hyperspectral satellite missions, such as EnMAP (Chabrillat et al., 2024) and PRISMA (Ward et al., 2024), and their derived soil products, which provide enhanced capabilities for topsoil SOC estimation.

For vegetation-derived carbon inputs, deviations tend to be relatively small in magnitude but less consistent in temporal behaviour, leading to lower nRMSE but reduced R^2. This sensitivity is primarily associated with limitations in biomass data

https://doi.org/10.5194/egusphere-2026-4735
Preprint. Discussion started: 9 September 2026

availability and challenges in accurately representing vegetation structure and productivity using remote-sensing-derived products. Currently, large-scale, well-validated biomass products remain less developed, although recent initiatives such as the European Space Agency biomass mission (https://earth.esa.int/eogateway/missions/biomass/biomass-data) are expected to improve data availability. In addition to data limitations, biomass estimation is further complicated by management-related factors. For example, in croplands, parcel-level crop type datasets from the European Land Parcel Identification System (LPIS; Milenov & Kay, 2006) provide a useful basis for estimating main crop production. However, management practices determining carbon inputs, particularly harvest residue management (i.e. whether residues are retained, incorporated, or removed), are generally unavailable at large spatial scales. Additional practices such as cover crops (Kathage et al., 2022; Poeplau & Don, 2015) are also rarely documented at large spatial scales, making them difficult to quantify their biomass contributions. Future improvements may be achieved through approaches that predict cover crop distributions (Fendrich et al., 2023; Zhou et al., 2025) and estimate their biomass (Goffart et al., 2021). Third, in heterogeneous systems such as agroforestry and forests, remote-sensing-derived biomass products may further struggle to represent complex vegetation structure and species composition. For example, relatively high nRMSE values were observed for vegetation-derived C input substitution in the agroforestry site SP-Agrofor-01 and even resulted in incorrect SOC change direction predictions. This is likely related to the high spatial heterogeneity of Mediterranean open woodland agroforestry systems, which are characterized by scattered trees, heterogeneous herbaceous cover, and variable shrub presence. Such vegetation structures can generate mixed remote-sensing signals and complicate the representation of site-specific biomass productivity. Similar challenges may also occur in forests with high species diversity and structurally complex canopies (Forrester et al., 2017). Together, these factors lead to inconsistencies in carbon input estimation and contribute to the observed sensitivity in SOC simulations.

Climate datasets are often considered relatively robust, but our results show that, although substituting in-situ climate data introduces relatively limited deviations in magnitude, it can still reduce the temporal coherence of model dynamics (R^2) in simulations. At DE-Crop-01, this effect was mainly driven by differences in water balance, with ERA5 providing higher rainfall and lower evaporation than the local climate station data. This reduced moisture limitation in RothC, increased decomposition rates, and consequently shifted the climate-driven simulation towards carbon-source behaviour, whereas the in-situ baseline indicated a carbon sink. A likely explanation is that remotely sensed or reanalysis climate data may smooth temporal variability, underestimate extreme events, introduce timing mismatches, or suffer from spatial representativeness errors, where localized rainfall events are not captured consistently by gridded climate products compared to in-situ observations (Jiang et al., 2021; Liu et al., 2024). Given the dependence of SOC decomposition on temperature and moisture, even small discrepancies in temporal patterns can propagate through the model and alter the shape of SOC trajectories.

4.2.2 Sensitivity structure and implications for post-processing strategies

Beyond quantifying the magnitude of sensitivity and improving input datasets prior to modelling, understanding the structure of sensitivity is essential for reducing the impacts of boundary-condition substitution through post-processing. An emerging strategy is to post-process SOC model outputs by recalibrating them against independent measurements or reference datasets

https://doi.org/10.5194/egusphere-2026-4735
Preprint. Discussion started: 9 September 2026

(Du et al., 2026; Ding et al., 2025). For example, the hybrid approach proposed by Zhang et al. (2024) combines process-based model outputs with machine learning to improve agreement with observations. In this framework, RothC-simulated SOC dynamics, together with auxiliary environmental covariates, are integrated into a random forest model to generate spatially explicit SOC products.

Our results provide a critical perspective on the applicability of such correction strategies, showing that their effectiveness depends strongly on the structure of the deviations between simulations and reference trajectories. When sensitivity is dominated by the SB component, post hoc correction is likely to be effective, as the deviation mainly represents a systematic offset and a stable mapping exists between modelled and reference SOC trajectories. This behaviour is typically observed at sites with low-quality initial SOC maps (e.g. BE-Grass-01, SP-Grass-02, SP-Forest-02), where MSD is dominated by SB (Fig. 6). In such cases, large offsets may mask the contributions of other boundary conditions and result in SOC trajectories that are nearly parallel to the baseline (Fig. A.2). As a result, this type of sensitivity can be readily corrected through post-processing. When NU dominates, correction may still be feasible if the relationship between trajectories remains monotonic and temporally stable. In contrast, LC reflects reduced temporal coherence and timing mismatches between simulations, which are inherently difficult to correct through post hoc calibration. This highlights limitation of hybrid correction frameworks and underscores the importance of diagnosing sensitivity types prior to applying post hoc bias-adjustment methods.

4.3 Implications of endpoint sensitivity and reporting window selection

4.3.1 Fixed endpoint sensitivity and the detectability of SOC changes and management effects

Fixed endpoint sensitivity provides a direct measure of the additional deviation introduced into estimated SOC change when site-specific boundary conditions are replaced by remote sensing derived spatial datasets. Across most study sites, annualized fixed endpoint sensitivity remained relatively small, with absolute values below 0.16 Mg C ha^{-1} yr^{-1}. Cropland sites generally exhibited smaller fixed endpoint sensitivities than forests and grasslands. However, cropland also showed substantially lower measured SOC change rates. Across our seven cropland sites, the mean absolute SOC change rate was approximately 0.31 Mg C ha^{-1} yr^{-1}, whereas the mean rate for the remaining land use types was approximately 0.99 Mg C ha^{-1} yr^{-1}. For most sites, annualized fixed endpoint sensitivity was smaller than the measured SOC change rate, suggesting that boundary-condition substitution introduces only limited additional deviations relative to the expected magnitude of SOC changes, and is therefore unlikely to largely compromise the predictive capability of process-based SOC models. These results support the use of remote sensing derived spatial datasets for regional-scale SOC assessments. Nevertheless, several sites exhibited considerably larger endpoint sensitivities. One approach to reducing these deviations is to improve the spatial datasets (Section 4.2.1). for the boundary conditions identified as the dominant contributors to endpoint sensitivity Alternatively, additional field observations may be collected for these sensitive boundary conditions or locations to reduce substitution uncertainty while maintaining the spatial scalability afforded by RS datasets.

https://doi.org/10.5194/egusphere-2026-4735
Preprint. Discussion started: 9 September 2026

The implications of endpoint sensitivity become even more important when evaluating management-induced SOC sequestration. Petersson et al. (2025) suggest that SOC sequestration achieved through widely promoted agricultural management practices is generally modest, typically ranging from 0.1 to 0.5 t C ha^{-1} yr^{-1}, including approximately 0.40 ± 0.32 t C ha^{-1} yr^{-1} for cover crops, 0.14 ± 0.06 t C ha^{-1} yr^{-1} for crop residue retention, 0.21 ± 0.16 t C ha^{-1} yr^{-1} for improved crop rotations, and 0.24 ± 0.34 t C ha^{-1} yr^{-1} for reduced tillage. At sites with high endpoint sensitivity, the deviations introduced by boundary-condition substitution may therefore be comparable to, or even exceed, the expected SOC gains attributable to these management practices. In such cases, substitution-induced sensitivity may mask or exaggerate estimates of management effectiveness. These findings highlight the importance of explicitly accounting for boundary-condition substitution sensitivity when process-based SOC models are used to evaluate carbon farming practices or support carbon accounting and Monitoring, Reporting and Verification (MRV) frameworks (Smith et al., 2020; Zhou et al., 2026).

4.3.2 Rolling endpoint sensitivity and reporting window selection

Besides the magnitude of endpoint sensitivity, its direction is equally important because it determines the inferred direction of SOC change and, consequently, whether a system is classified as a carbon sink or a carbon source. The reporting window further influences this interpretation by controlling the balance between short-term variability and long-term accumulation effects, thereby affecting both the magnitude and direction of inferred SOC change.

The rolling window analysis shows that short reporting periods are highly sensitive to variability introduced by boundary-condition substitution. This is especially evident in cropland systems, where SOC changes are typically small and may fluctuate around zero (Fig. 3). In such cases, even minor differences in slope or temporal coherence can lead to incorrect classifications of SOC change direction. For example, substitution of vegetation-derived carbon inputs at IT-Crop-02 introduces substantial LC components, resulting in a reversed SOC change direction over short reporting windows and misclassification of the system as a carbon sink. As the reporting window increases, the cumulative SOC change signal progressively exceeds short-term variability, leading to more stable and directionally consistent estimates. However, longer reporting windows do not mean more reliable results. Fixed endpoint analysis shows that increasing the simulation period amplifies the cumulative effects of boundary-condition sensitivity, often leading to overestimation of SOC change.

These findings suggest that conclusions about whether a system acts as a carbon sink or source are not solely determined by underlying system dynamics, but are also influenced by model behaviour, the quality of substituted remote sensing inputs, and the design of the reporting framework. This includes a sensitivity to the length of the reporting window: shorter windows tend to be more affected by short-term variability, whereas longer windows increasingly reflect the accumulation of model deviations. Based on our results, a reporting window of approximately 15–30 years appears to provide a practical compromise between these two effects.

We summarized several large-scale studies that use SOC modelling frameworks combining process-based models with remote sensing inputs (Table 4). Among studies aiming to report SOC change, most adopt simulation periods that are longer than

https://doi.org/10.5194/egusphere-2026-4735
Preprint. Discussion started: 9 September 2026

those suggested by our findings, with only one study adopting a reporting window consistent with our recommendations. In carbon accounting and management assessment, excessively long reporting windows (>30 years) can lead to larger deviations from baseline simulations. While long-term simulations are essential for understanding system behaviour, they accumulate sensitivity effects and deviations over time, making them less suitable for directly quantifying SOC change for reporting purposes. More generally, reporting frameworks should account for the interaction between model sensitivity and temporal evolution, rather than treating endpoint estimates as inherently robust indicators of SOC change. Before evaluating a system as a carbon sink or source in SOC reporting and carbon accounting, the reporting period should be carefully considered.

Table 4. Summary of recent large-scale SOC modelling studies using process-based models and remote sensing inputs.

Scale	Land use	Depth	Model	Simulation period	Length	purpose	Source
Global	All	30 cm	RothC	2014-2100	86	Projection	Morais et al. (2019)
Global	All	30 cm	RothC	2020-2040	20	Projection	GSOCseq; FAO (2022)
Global	agriculture	30 cm	RothC	1919-2018	100	Reporting	Poeplau & Dechow (2023)
Australia	All	30 cm	MIMICS	1991-2020	30	Prediction	Wang et al. (2024)
UK	agriculture	30 cm	RothC	2020-2050	30	Projection	Jordon et al. (2022)
Denmark	agriculture	20 cm	RothC	2018-2038	20	Projection	Gutierrez et al. (2023)
Lithuania	agriculture	20 cm	RothC	2020-2022 2022-2042	3 20	Reporting Projection	Samarinas et al., (2025)
China	agriculture	30 cm	RothC	1980-2020	40	Reporting	Lin et al. (2024)
China	black soil cropland	30 cm	RothC-AutoML	1980-2023 2023-2100	43 77	Reporting Projection	Chen et al., (2026)

In addition, as can be seen from the Table 4, lots of studies are designed for projection which SOC simulations extending to several decades or even centuries in future under different climate and management scenarios. These simulation horizons should not be conflated with reporting windows used for endpoint-based SOC change assessment, we did not evaluate the reasonableness of their simulation period, because we cannot compare future data products with in-situ datasets. Meantime, we did not consider simulations using Earth System Models (ESMs), which are commonly applied at much coarser spatial resolutions, often at grid scales over long time horizons. SOC dynamics in ESMs are highly aggregated and involves different ecosystem processes and objectives compared to the modelling frameworks considered here.

5 Conclusion

This study develops a general framework for quantifying boundary-condition sensitivity in SOC modelling in the context of replacing in-situ inputs with remote sensing–derived data, distinguishing between dynamic and endpoint sensitivity.

Our results show that sensitivity cannot be adequately captured from a single perspective, as different boundary conditions and metrics reflect different aspects of model behaviour. In particular, initial SOC stock, vegetation-derived carbon inputs and climate products emerged as dominant sources of dynamic sensitivity. Fixed endpoint sensitivity was generally small relative to the magnitude of measured SOC changes, supporting the use of remote sensing and remote sensing-derived spatial datasets

https://doi.org/10.5194/egusphere-2026-4735
Preprint. Discussion started: 9 September 2026

as scalable boundary-condition proxies for regional SOC modelling. Another key finding is that endpoint-based assessments are strongly dependent on the reporting window. The choice of time horizon determines the balance between short-term noise and long-term accumulation effects and can influence both the magnitude and direction of SOC change. In systems with small SOC changes, such as croplands, inappropriate reporting windows may even lead to incorrect conclusions regarding carbon sink or source behaviour.

These findings have important implications for large-scale SOC modelling and carbon accounting. They highlight the need to explicitly consider sensitivity structure, prioritise critical input variables, and carefully select reporting windows when interpreting model outputs. Together, this work provides a basis for more transparent and robust SOC assessments in the context of increasing reliance on remote sensing data.

https://doi.org/10.5194/egusphere-2026-4735
Preprint. Discussion started: 9 September 2026

Appendix A Figures and Tables

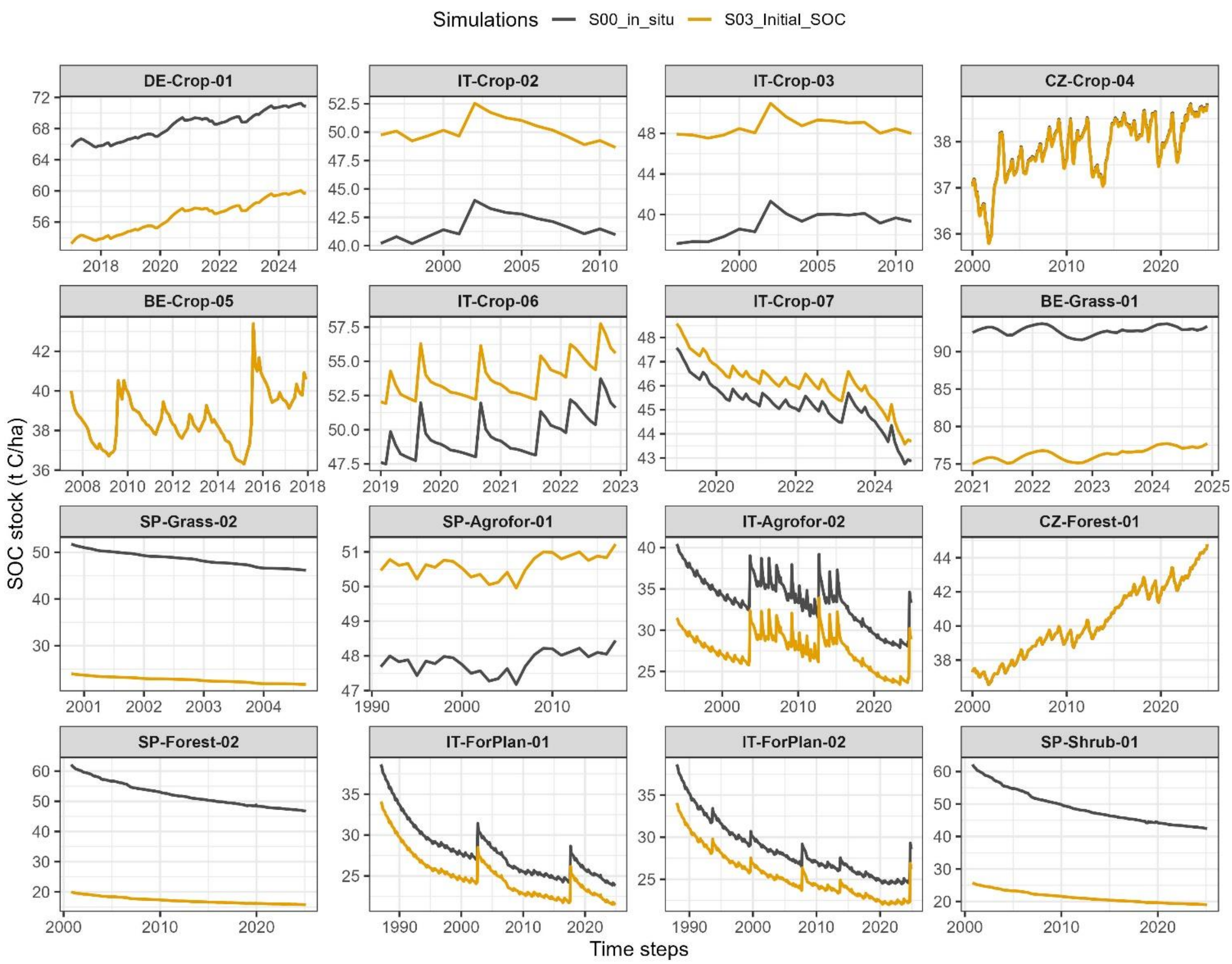

585

Fig.A.1. Comparison of SOC time series between *S00_in_situ* and *S03_Initial_SOC* across all sites.

https://doi.org/10.5194/egusphere-2026-4735
Preprint. Discussion started: 9 September 2026

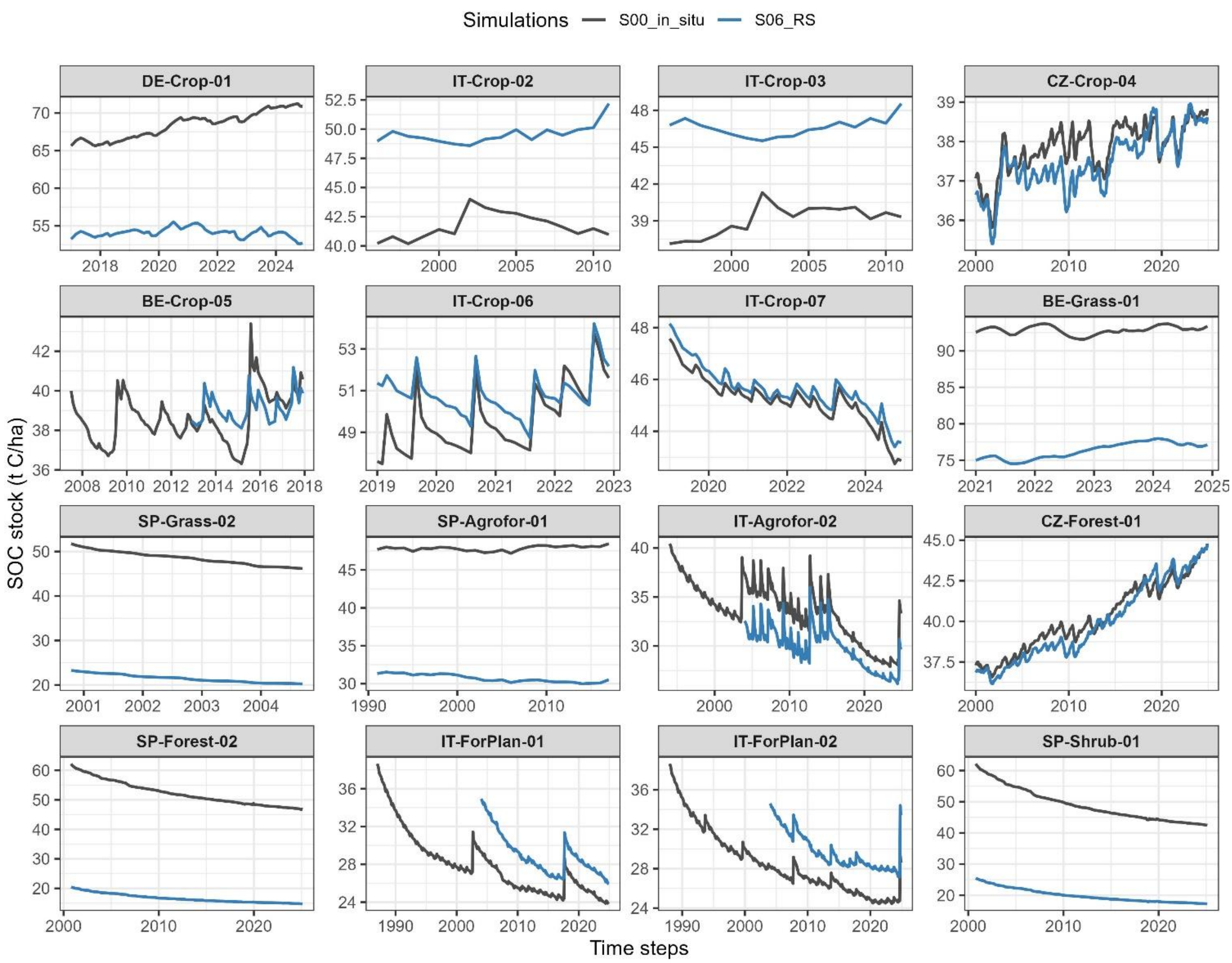

Fig.A.2. Comparison of SOC time series between *S00_in_situ* and *S06_RS* across all sites.

Appendix B Detailed explanation of boundary condition preparation

Appendix B.1 CASA model

Spatially explicit yield estimates were derived from dekadal (10-day) net primary productivity (NPP) data using the Carnegie–Ames–Stanford Approach (CASA) model (Potter et al., 1993). The CASA model is based on a light use efficiency (LUE) framework and has been widely applied to estimate NPP and carbon storage across multiple spatial scales (Fang et al., 2021; Pei et al., 2022). In this study, NPP was calculated following the standard CASA processing workflow, with several modifications to improve performance for cropland systems. In particular, NDVI saturation effects in crop biomass estimation

https://doi.org/10.5194/egusphere-2026-4735
Preprint. Discussion started: 9 September 2026

were mitigated by using the Sentinel-2 leaf area index (LAI) proxy (SeLI), derived from red-edge bands (Pasqualotto et al., 2019). In addition, dekadal albedo dynamics were incorporated into the estimation of photosynthetically active radiation (PAR) by adapting formulations originally developed for Landsat-8/9 to Sentinel-2 data (He et al., 2018). NPP values were converted to aboveground biomass (AGB) using empirical relationships calibrated against ground-truth dry AGB data from the long-term experimental (LTE) sites.

Appendix B.2 Calculate C input based on livestock numbers

For regional simulations, carbon inputs from organic amendments were estimated based on livestock statistics at the provincial level. Annual manure production for each livestock type was first calculated using livestock numbers (typically obtained from national statistical offices) and species-specific manure production rates derived from the literature (e.g. Scarlat et al., 2018). The total carbon input was then derived by converting manure amounts (fresh weight) into carbon content, accounting for the distribution of manure across different management systems (e.g. solid storage, liquid slurry, and on-pasture deposition; IPCC, 2019, Tables 10A.6–10A.9) and their corresponding carbon content ratios (e.g. Hendriks et al., 2023). Finally, total carbon inputs from organic amendments were spatially allocated by assuming an even distribution across agricultural areas within each province and expressed as average carbon input per unit area. A more detailed description of the algorithms and parameterization is provided in Zhou et al. (2026, under review).

Code and data availability

All source code used in this study is publicly available via Zenodo (DOI: 10.5281/zenodo.21644168). The data required to reproduce the analyses are available to reviewers upon request during the review process. All remote sensing datasets generated within the MRV4SOC project (https://mrv4soc.eu/) are currently under preparation and will be published in a FAIR-compliant public repository with a DOI after completion of the project.

Author contributions

BG, BvW, and MGG conceived and designed the study and secured the project funding. YZ developed the methodology, performed the analyses, and wrote the original draft of the manuscript. JT, LHM, JBG, MS, DC, DFB, RM, and MF contributed to the methodological development of the modelling framework. All authors contributed to data curation, manuscript review and editing, and approved the final version.

https://doi.org/10.5194/egusphere-2026-4735
Preprint. Discussion started: 9 September 2026

Competing interests

Bas van Wesemael is a member of the editorial board of SOIL.

Financial support

This paper is part of the MRV4SOC project funded by the European Union' s Horizon Europe Research and Innovation Action program under Grant Agreement No. 101112754. Funded by the European Union. Views and opinions expressed are however those of the author(s) only and do not necessarily reflect those of the European Union or European Research Executive Agency (REA). Neither the European Union nor the granting authority can be held responsible for them.

References

Abatzoglou, J., Dobrowski, S., Parks, S., Hegewisch, K., 2018. TerraClimate, a high-resolution global dataset of monthly climate and climatic water balance from 1958–2015. Sci Data 5, 170191. https://doi.org/10.1038/sdata.2017.191

Angelopoulou, T., Tziolas, N., Balafoutis, A., Zalidis, G., and Bochtis, D. 2019. Remote sensing techniques for soil organic carbon estimation: A review. Remote Sensing, 11(6), 676. https://doi.org/10.3390/rs11060676

Arrouays, D., McBratney, A., Bouma, J., Libohova, Z., Richer-de-Forges, A., Morgan, C., Roudier, P., Poggio, L. and Mulder, V., 2020. Impressions of digital soil maps: The good, the not so good, and making them ever better. Geoderma Regional, 20, p.e 00255.

Bolinder, M.A., Janzen, H.H., Gregorich, E.G., Angers, D.A., VandenBygaart, A.J. 2007. An approach for estimating net primary productivity and annual carbon inputs to soil for common agricultural crops in Canada. Agric. Ecosyst. Environ., 118(1–4), 29-42.

Brell, M., Spengler, D., Ruhtz, T., Ward, K., Chabrillat, S., Segl, K., Foerster, S., and Itzerott, S. 2020. Demmin, Germany (October 2015) - an EnMAP Preparatory Flight Campaign. GFZ Data Services. https://doi.org/10.5880/enmap.2020.004

Bruni, E., Lugato, E., Chenu, C., and Guenet, B. 2024. European croplands under climate change: Carbon input changes required to increase projected soil organic carbon stocks. Science of The Total Environment, 954, 176525. https://doi.org/10.1016/j.scitotenv.2024.176525

Castaldi, F., Syu, C.-H., Valdez, M. C., Yen, C.-C., Chen, C.-F., Bertinaria, F., and Toscano, P. 2026. Monitoring soil organic carbon from earth observation in the era of cover cropping and no-tillage. Smart Agricultural Technology, 13, 101935. https://doi.org/10.1016/j.atech.2026.101935

Černý, M., Pařez, J., Malík, V. 1996. Růstové a taxační tabulky hlavních dřevin České republiky. Jílové u Prahy: IFER.

Chabrillat, S., Ben-Dor, E., Cierniewski, J., Gomez, C., Schmid, T., and van Wesemael, B. 2019. Imaging Spectroscopy for Soil Mapping and Monitoring, Surveys in Geophysics, 40(3), 361-399, https://doi.org/10.1007/s10712-019-09524-0

https://doi.org/10.5194/egusphere-2026-4735
Preprint. Discussion started: 9 September 2026

Chabrillat, S., Foerster, S., Segl, K., Beamish, A., Brell, M., Asadzadeh, S., Milewski, R., Ward, K.J., Brosinsky, A., Koch, K., Scheffler, D., Guillaso, S., Kokhanovsky, A., Roessner, S., Guanter, L., Kaufmann, H., Pinnel, N., Carmona, E., Storch, T., Hank, T., Berger, K., Wocher, M., Hostert, P., van der Linden, S., Okujeni, A., Janz, A., Jakimow, B., Bracher, A., Soppa, M.A., Alvarado, L.M.A., Buddenbaum, H., Heim, B., Heiden, U., Moreno, J., Ong, C., Bohn, N., Green, R.O., Bachmann, M., Kokaly, R., Schodlok, M., Painter, T.H., Gascon, F., Buongiorno, F., Mottus, M., Brando, V.E., Feilhauer, H., Betz, M., Baur, S., Feckl, R., Schickling, A., Krieger, V., Bock, M., La Porta, L., Fischer, S., 2024. The EnMAP spaceborne imaging spectroscopy mission: Initial scientific results two years after launch. Remote Sensing of Environment 315, 114379. https://doi.org/10.1016/j.rse.2024.114379

Chen, J., Hu, W., Xu, X., Tong, Y., Yan, G., Yu, D., Zhao, Y., Ma, L., Xie, E., Zhang, Y., Zou, T., Jia, Z., Thompson, M.L., Taboada, M.A., Zhao, Y., 2026. Organic carbon loss from the black soil region threatens food security in China. The Innovation Geoscience 4(2), 100213.

Chen, S., Arrouays, D., Leatitia Mulder, V., Poggio, L., Minasny, B., Roudier, P., Libohova, Z., Lagacherie, P., Shi, Z., Hannam, J., Meersmans, J., Richer-de-Forges, A.C., Walter, C., 2022. Digital mapping of GlobalSoilMap soil properties at a broad scale: A review. Geoderma 409, 115567.

Choi, W., Ryu, Y., Kong, J., Jeong, S., and Lee, K. 2025. Evaluation of spatial and temporal variability in Sentinel-2 surface reflectance on a rice paddy landscape. Agricultural and Forest Meteorology, 363, 110401. https://doi.org/10.1016/j.agrformet.2025.110401

Coleman, K., Jenkinson, D.S., 1996. RothC-26.3 - A Model for the turnover of carbon in soil. In: Powlson, D.S., Smith, P., Smith, J.U. (Eds.), Evaluation of Soil Organic Matter Models. Springer Berlin Heidelberg, 237-246.

Ding, Z., Liu, K., Grunwald, S., Smith, P., Ciais, P., Wang, B., Wadoux, A.M.J.C., Ferreira, C., Karunaratne, S., Shurpali, N., Yin, X., Roberts, D., Madgett, O., Duncan, S., Zhou, M., Liu, Z., Harrison, M.T., 2025. Advancing Soil Organic Carbon Prediction: A Comprehensive Review of Technologies, AI, Process-Based and Hybrid Modelling Approaches. Adv. Sci. 12, e04152.

Du, Y., Minasny, B., Ng, W., Zhang, L., Saby, N.P.A., Zhou, Y., van Wesemael, B., Ma, Y., Wang, Z., Luo, Z., Shi, Z., Chen, S., 2026. Spatiotemporal modelling of soil organic carbon: Integrating process-based and machine learning approaches. Geoderma 473, 117967. https://doi.org/10.1016/j.geoderma.2026.117967.

Ellis, E., Paustian, K. 2024. Importance of on-farm research for validating process-based models of climate-smart agriculture. Carbon Balance Manage 19, 16. https://doi.org/10.1186/s13021-024-00260-6

FAO, 2020. Technical specifications and country guidelines for Global Soil Organic Carbon Sequestration Potential Map (GSOCseq). Rome.

FAO. 2022. Global Soil Organic Carbon Sequestration Potential Map – GSOCseq v.1.1. Technical report. Rome. https://doi.org/10.4060/cb9002en

Fang, P., Yan, N., Wei, P., Zhao, Y., Zhang, X. 2021. Aboveground Biomass Mapping of Crops Supported by Improved CASA Model and Sentinel-2 Multispectral Imagery. Remote Sensing, 13(14). https://doi.org/10.3390/rs13142755

Farina, R., Coleman, K., Whitmore, A.P., 2013. Modification of the RothC model for simulations of soil organic C dynamics in dryland regions. Geoderma 200–201, 18–30. https://doi.org/10.1016/j.geoderma.2013.01.021

Fendrich, A.N., Matthews, F., Van Eynde, E., Carozzi, M., Li, Z., d'Andrimont, R., Lugato, E., Martin, P., Ciais, P., Panagos, P., 2023. From regional to Parcel Scale: A high-resolution map of cover crops across Europe combining satellite data with statistical surveys. Sci. Total Environ. 873, 162300

Field, C. B., Randerson, J. T., Malmström, C. M. 1995. Global net primary production: Combining ecology and remote sensing. Remote Sensing of Environment, 51(1), 74–88. https://doi.org/10.1016/0034-4257(94)00066-v

Filipiak, M., Gabriel, D., Kuka, K. 2023. Simulation-based assessment of the soil organic carbon sequestration in grasslands in relation to management and climate change scenarios. Heliyon, 9(6), e17287.

Forrester, D.I., Tachauer, I.H.H., Annighoefer, P., Barbeito, I., Pretzsch, H., Ruiz-Peinado, R., Stark, H., Vacchiano, G., Zlatanov, T., Chakraborty, T., Saha, S., Sileshi, G.W., 2017. Generalized biomass and leaf area allometric equations for European tree species incorporating stand structure, tree age and climate. Forest Ecology and Management 396, 160–175.

Gauch, Hugh G., J. T. Gene Hwang, and Gary W. Fick. 2003. Model Evaluation by Comparison of Model-Based Predictions and Measured Values. Agronomy Journal 95(6): 1442–46. doi:10.2134/agronj2003.1442.

Geremew, B., Tadesse, T., Bedadi, B., Gollany, H. T., Tesfaye, K., Aschalew, A., Tilaye, A., Abera, W. 2024. Evaluation of RothC model for predicting soil organic carbon stock in north-west Ethiopia. Environmental Challenges, 15, 100909. https://doi.org/10.1016/j.envc.2024.100909

Goffart, D., Curnel, Y., Planchon, V., Goffart, J.P., Defourny, P. 2021. Field-scale assessment of Belgian winter cover crops biomass based on Sentinel-2 data. Eur. J. Agron. 126, 126278. https://doi.org/10.1016/j.eja.2021.126278

Gutierrez, S., Grados, D., Møller, A.B., de Carvalho Gomes, L., Beucher, A.M., Giannini-Kurina, F., de Jonge, L.W., Greve, M.H., 2023. Unleashing the sequestration potential of soil organic carbon under climate and land use change scenarios in Danish agroecosystems. Science of The Total Environment 905, 166921. https://doi.org/10.1016/j.scitotenv.2023.166921

Hendriks, C., Lesschen, J.P., Timmermans, B., Hanegraaf, M., Dijkman, W., Rougoor, C., Cruijsen, J., Schepens, J., 2023. Description and development Soil Carbon Tool. Wageningen: Slim Landgebruik

Hersbach, H., Bell, B., Berrisford, P., Hirahara, S., Horányi, A., Muñoz-Sabater, J., Nicolas, J., Peubey, C., Radu, R., Schepers, D., Simmons, A., Soci, C., Abdalla, S., Abellan, X., Balsamo, G., Bechtold, P., Biavati, G., Bidlot, J., Bonavita, M., De Chiara, G., Dahlgren, P., Dee, D., Diamantakis, M., Dragani, R., Flemming, J., Forbes, R., Fuentes, M., Geer, A., Haimberger, L., Healy, S., Hogan, R.J., Hólm, E., Janisková, M., Keeley, S., Laloyaux, P., Lopez, P., Lupu, C., Radnoti, G., de Rosnay, P., Rozum, I., Vamborg, F., Villaume, S., Thépaut, J.-N., 2020. The ERA5 global reanalysis. Quarterly Journal of the Royal Meteorological Society 146, 1999–2049.

He, T., Liang, S., Wang, D., Cao, Y., Gao, F., Yu, Y., & Feng, M. (2018). Evaluating land surface albedo estimation from Landsat MSS, TM, ETM+, and OLI data based on the unified direct estimation approach. Remote Sensing of Environment, 204, 181–196. https://doi.org/https://doi.org/10.1016/j.rse.2017.10.031

Huang, H., Yang, L., Zhang, L., Pu, Y., Yang, C., Wu, Q., Cai, Y., Shen, F., Zhou, C., 2022. A review on digital mapping of soil carbon in cropland: Progress, challenge, and prospect. Environmental Research Letters 17(12), 123004. https://doi.org/10.1088/1748-9326/aca41e

IPCC. 2006. 2006 IPCC Guidelines for National Greenhouse Gas Inventories. Prepared by the National Greenhouse Gas Inventories Programme, Eggleston, H.S., Buendia, L., Miwa, K., Ngara, T. and Tanabe, K. (eds). IGES, Japan.

IPCC, 2019. 2019 Refinement to the 2006 IPCC Guidelines for National Greenhouse Gas Inventories, eds. E. Calvo Buendia, K. Tanabe, A. Kranjc, J. Baasansuren, M. Fukuda, S. Ngarize, A. Osako, Y. Pyrozhenko, P. Shermanau, S. Federici. IPCC, Switzerland.

Itzerott, S., Hohmann, C., Stender, V., Maass, H., Borg, E., Renke, F., Jahncke, D., Berg, M., Conrad, C., and Spengler, D. 2018. TERENO (Northeast), Climate stations of the GFZ German Research Centre for Geosciences (GFZ) (Version 2.0). GFZ Data Services. https://doi.org/10.5880/TERENO.GFZ.CL.2018.ALL

Jiang, Q., Li, W., Fan, Z., He, X., Sun, W., Chen, S., Wen, J., Gao, J., Wang, J., 2021. Evaluation of the ERA5 reanalysis precipitation dataset over Chinese Mainland. Journal of Hydrology 595, 125660.

Jordon, M.W., Smith, P., Long, P.R., Bürkner, P.C., Petrokofsky, G., Willis, K.J., 2022. Can Regenerative Agriculture increase national soil carbon stocks? Simulated country-scale adoption of reduced tillage, cover cropping, and ley-arable integration using RothC. Sci. Total Environ. 825(153955).

Karger, D.N., Conrad, O., Böhner, J., Kawohl, T., Kreft, H., Soria-auza, R.W., Zimmermann, N.E., Linder, H.P., Kessler, M., 2017. Climatologies at high resolution for the earth's land surface areas. Sci Data 4, 170122. https://doi.org/10.1038/sdata.2017.122

Kathage, J., Smit, B., Janssens, B., Haagsma, W., Adrados, J.L., 2022. How much is policy driving the adoption of cover crops? Evidence from four EU regions. Land Use Policy 116, 106016. https://doi.org/10.1016/j.landusepol.2022.106016

Lagacherie, P., Arrouays, D., Bourennane, H., Gomez, C., Nkuba-Kasanda, L., 2020. Analysing the impact of soil spatial sampling on the performances of digital soil mapping models and their evaluation: A numerical experiment on quantile random forest using clay contents obtained from Vis–NIR–SWIR hyperspectral imagery. Geoderma 375, 114503.

Lai, Y., Mulder, V.L., Heuvelink, G.B.M., Kros, H., Ros, G.H. 2026. A RothC-based spatiotemporal analysis of soil organic carbon stocks in agricultural soils of the Netherlands (1986–2022). Geoderma, 467, 117753.

Lal, R. 2004. Soil carbon sequestration to mitigate climate change. Geoderma, 123, 1–22.

Le Noë, J., Manzoni, S., Abramoff, R., Bölscher, T., Bruni, E., Cardinael, R., Ciais, P., Chenu, C., Clivot, H., Derrien, D., Ferchaud, F., Garnier, P., Goll, D., Lashermes, G., Martin, M., Rasse, D., Rees, F., Sainte-Marie, J., Salmon, E., Schiedung, M., Schimel, J., Wieder, W., Abiven, S., Barré, P., and Guenet, B. 2023. Soil organic carbon models need independent time-series validation for reliable prediction. Communications Earth & Environment, 4, 158. https://doi.org/10.1038/s43247-023-00797-6

https://doi.org/10.5194/egusphere-2026-4735
Preprint. Discussion started: 9 September 2026

Lin, Z., Lu, X., Xu, Y., Sun, W., Yu, Y., Zhang, W., Mishra, U., Kuzyakov, Y., Wang, G., Qin, Z., 2024. Increased straw return promoted soil organic carbon accumulation in China's croplands over the past 40 years. Science of The Total Environment 945, 173903. https://doi.org/10.1016/j.scitotenv.2024.173903

Liu, F., Wu, H., Zhao, Y., Li, D., Yang, J.-L., Song, X., Shi, Z., Zhu, A.-X., Zhang, G.-L., 2022. Mapping high resolution national soil information grids of China. Science Bulletin 67(3), 328–340.

Liu, R., Zhang, X., Wang, W., Wang, Y., Liu, H., Ma, M., Tang, G., 2024. Global-scale ERA5 product precipitation and temperature evaluation. Ecological Indicators 166, 112481.

McBratney, A.B., Mendonca Santos, M.L., Minasny, B., 2003. On digital soil mapping. Geoderma 117, 3–52. https://doi.org/10.1016/S0016-7061(03)00223-4.

Menéndez-Miguélez, M., Calama, R., Del Río, M., Madrigal, G., López-Senespleda, E., Pardos, M., Ruiz-Peinado, R., 2022. Species-specific and generalized biomass models for estimating carbon stocks of young reforestations. Biomass Bioenergy 161, 106453.

Milenov, P and Kay, S., 2006. Status of the Implementation of LPIS in the EU Member States, Proceedings of the 12th MARS PAC Annual Conference, 27–29 November 2006, Toulouse, France.

Minasny, B., Malone, B. P., McBratney, A. B., Angers, D. A., Arrouays, D., Chambers, A., Chaplot, V., Chen, Z.-S., Cheng, K., Das, B. S., Field, D. J., Gimona, A., Hedley, C. B., Hong, S. Y., Mandal, B., Marchant, B. P., Martin, M., McConkey, B. G., Mulder, V. L., O'Rourke, S., Richer-de-Forges, A. C., Odeh, I., Padarian, J., Paustian, K., Pan, G., Poggio, L., Savin, I., Stolbovoy, V., Stockmann, U., Sulaeman, Y., Tsui, C.-C., Vågen, T.-G., van Wesemael, B., & Winowiecki, L. 2017. Soil carbon 4 per mille. Geoderma, 292, 59–86. https://doi.org/10.1016/j.geoderma.2017.01.002.

Morais TG, Teixeira RF, Domingos T. 2019. Detailed global modelling of soil organic carbon in cropland, grass and forest soils. PLoS ONE 14(9): e0222604. https://doi-org.insu.bib.cnrs.fr/10.1371/journal.pone.0222604

Morais, T.G., Teixeira, R.F., Domingos, T. 2019. Detailed global modelling of soil organic carbon in cropland, grassland and forest soils. PLoS ONE, 14(9), e0222604. https://doi.org/10.1371/journal.pone.0222604

Pasalodos-Tato, M., Ruiz-Peinado, R., del Río, M., Montero, G., 2015. Shrub biomass accumulation and growth rate models to quantify carbon stocks and fluxes for the Mediterranean region. Eur. J. For. Res. 134, 537–553. https://doi.org/10.1007/s10342-015-0870-6

Palantza, D., Karyotis, K., Campo, J. T. F. d., Mateo, L. H., Zalidis, G. 2026. Remote Sensing and AI-Based Monitoring of Soil Properties for Tier-3 MRV Framework of Complex Mediterranean Agroforestry Systems. Remote Sens. 18(13), 2077. https://doi.org/10.3390/rs18132077

Paustian, K., Lehmann, J., Ogle, S., Reay, D., Robertson G.P., Smith P. 2016. Climate-smart soils. Nature, 532, 49–57.

Petersson, T., Antoniella, G., Perugini, L., Chiriacò, M.V., Chiti, T., 2025. Carbon farming practices for European cropland: A review on the effect on soil organic carbon. Soil & Tillage Research 247, 106353. https://doi.org/10.1016/j.still.2024.106353

Pei, Y., Dong, J., Zhang, Y., Yuan, W., Doughty, R., Yang, J., Zhou, D., Zhang, L., Xiao, X. 2022. Evolution of light use efficiency models: Improvement, uncertainties, and implications. Agricultural and Forest Meteorology, 317, 108905. https://doi.org/https://doi.org/10.1016/j.agrformet.2022.108905

Poeplau, C. 2016. Estimating root: shoot ratio and soil carbon inputs in temperate grasslands with the RothC model. Plant Soil. 407, 293–305. https://doi.org/10.1007/s11104-016-3017-8

Poeplau, C., Dechow, R. 2023. The legacy of one hundred years of climate change for organic carbon stocks in global agricultural topsoils. Sci. Rep., 13, 7483.

Poeplau, C., Don, A. 2015. Carbon sequestration in agricultural soils via cultivation of cover crops – A meta-analysis. Agric. Ecosyst. Environ., 200, 33-41.

Poggio, L., de Sousa, L.M., Batjes, N.H., Heuvelink, G.B.M., Kempen, B., Ribeiro, E., Rossiter, D., 2021. SoilGrids 2.0: producing soil information for the globe with quantified spatial uncertainty. SOIL 7, 217–240. https://doi.org/10.5194/soil-7-217-2021.

Potter, C.S., Randerson, J.T., Field, C.B., Matson, P.A., Vitousek, P.M., Mooney, H.A., Klooster, S.A. 1993. Terrestrial ecosystem production: A process model based on global satellite and surface data. Global Biogeochemical Cycles, 7, 811–841.

Pretzsch, H., Biber, P., Durský, J. 2014. The single tree-based stand simulator SILVA: construction, application and evaluation. Forest Ecology and Management, 162(1), 3-21. DOI: 10.1016/S0378-1127(02)00047-6.

Ruiz-Peinado, R., Rio, M., Montero, G., 2011. New models for estimating the carbon sink capacity of Spanish softwood species. For. Syst. 20, 176–188.

Safanelli, J.L., Chabrillat, S., Ben-Dor, E., Demattê, J.A., 2020. Multispectral models from bare soil composites for mapping topsoil properties over Europe. Remote Sens. 12, 1369.

Samarinas, N., Tsakiridis, N.L., Kalopesa, E., Tziolas, N., 2025. An agricultural hybrid carbon model for national-scale SOC stock spatial estimation. Environments 12(12), 477. https://doi.org/10.3390/environments12120477

Scarlat, N., Fahl, F., Dallemand, J.-F., Monforti, F., Motola, V., 2018. A spatial analysis of biogas potential from manure in Europe. Renew. Sustain. Energy Rev. 94 (915-930). https://doi.org/10.1016/j.rser.2018.06.035

Smith, P., Soussana, J.-F., Angers, D., Schipper, L., Chenu, C., Rasse, D.P., Batjes, N.H., van Egmond, F., McNeill, S., Kuhnert, M., Arias-Navarro, C., Olesen, J.E., Chirinda, N., Fornara, D., Wollenberg, E., Álvaro-Fuentes, J., Sanz-Cobena, A., Klumpp, K. 2020. How to measure, report and verify soil carbon change to realize the potential of soil carbon sequestration for atmospheric greenhouse gas removal. Glob. Change Biol. 25, 1906–1924. https://doi.org/10.1111/gcb.14815.

Studdert, G.A., Monterubbianesi, M.G., Domínguez, G.F., 2011. Use of RothC to simulate changes of organic carbon stock in the arable layer of a Mollisol of the southeastern Pampas under continuous cropping. Soil and Tillage Research 117, 191–200.

Stumpf, F., Behrens, T., Schmidt, K., Keller, A., 2024. Exploiting soil and remote sensing data archives for 3D mapping of multiple soil properties at the Swiss national scale. Remote Sensing 16(15), 2712.

https://doi.org/10.5194/egusphere-2026-4735
Preprint. Discussion started: 9 September 2026

Torres, J., Cañellas, I., Moreno-Fernández, D., González, I., Moreno, G., Guenet, B., Gómez-Giménez, M., Gimeno, B, Santín, I., Hernández-Mateo, L., 2026. Management legacies and forest attributes shape soil organic carbon dynamics in Quercus ilex open woodlands. Forest Ecology and Management 621, 124216. https://doi.org/10.1016/j.foreco.2026.124216

Tran, B. N., van der Kwast, J., Seyoum, S., Uijlenhoet, R., Jewitt, G., and Mul, M. 2023. Uncertainty assessment of satellite remote-sensing-based evapotranspiration estimates: a systematic review of methods and gaps. Hydrology and Earth System Sciences, 27, 4505–4528. https://doi.org/10.5194/hess-27-4505-2023

van Wesemael, B., Abdelbaki, A., Ben-Dor, E., Chabrillat, S., d'Angelo, P., Demattê, J.A.M., Genova, G., Gholizadeh, A., Heiden, U., Karlshoefer, P., Milewski, R., Poggio, L., Sabetizade, M., Sanz, A., Schwind, P., Tsakiridis, N., Tziolas, N., Yagüe, J., Žížala, D. 2024, European soil organic carbon monitoring system leveraging Sentinel 2 imagery and the LUCAS soil data base, Geoderma, 452, 117113. https://doi.org/10.1016/j.geoderma.2024.117113

Ward, K.J., Chabrillat, S., Foerster, S. 2024, Estimating Soil Organic Carbon using multitemporal PRISMA imaging spectroscopy data, Geoderma 450, 117025. https://doi.org/10.1016/j.geoderma.2024.117025

Wang, L., Abramowitz, G., Wang, Y.-P., Pitman, A., Viscarra Rossel, R.A., 2024. An ensemble estimate of Australian soil organic carbon using machine learning and process-based modelling. SOIL 10, 619–636. https://doi.org/10.5194/soil-10-619-2024

Wang, Z., Zhao, R., Xue, J., Lu, R., Chen, Z., Yu, Q., Chen, W., Zhang, Q., Shi, Z., Chen, S., 2026. A preliminary comparison of SOC storage between the traditional farmland and well-facilitated farmland management. Earth's Future, 14, e2025EF007810.

Warm Winter 2020 Team, ICOS Ecosystem Thematic Centre, 2022. Warm Winter 2020 ecosystem eddy covariance flux product for 73 stations in FLUXNET-Archive format—release 2022-1. https://doi.org/10.18160/2G60-ZHAK

Wiesmeier, M., Poeplau, C., Sierra, C.A., Maier, H., Frühauf, C., Hübner, R., Kühnel, A., Spörlein, P., Geuß, U., Hangen, E., Schilling, B., von Lützow, M., Kögel-Knabner, I. 2016. Projected loss of soil organic carbon in temperate agricultural soils in the 21st century: effects of climate change and carbon input trends. Scientific Reports, 6, Article 32525. https://doi.org/10.1038/srep32525

Wiltshire, S., Clemins, P. J., and Beckage, B. 2024. Granularity of model input data impacts estimates of carbon storage in soils. PLOS Climate, 3(10), e0000363. https://doi.org/10.1371/journal.pclm.0000363

Wu, H., and Li, Z.-L. 2009. Scale issues in remote sensing: A review on analysis, processing and modeling. Sensors, 9(3), 1768–1793. https://doi.org/10.3390/s90301768

Zhang, L., Heuvelink, G.B.M., Mulder, V.L., Chen, S., Deng, X., Yang, L., 2024. Using process-oriented model output to enhance machine learning-based soil organic carbon prediction in space and time. Sci. Total Environ. 922, 170778.

Zhou, Y., Chartin, C., Van Oost, K., van Wesemael, B., 2022. High-resolution soil organic carbon mapping at the field scale in southern Belgium (Wallonia). Geoderma. 422, 115929. https://doi.org/10.1016/j.geoderma.2022.115929

https://doi.org/10.5194/egusphere-2026-4735
Preprint. Discussion started: 9 September 2026

Zhou, Y., Ferdinand, M.S., Van Wesemael, J., Dvorakova, K., Baret, P.V., Van Oost, K., Van Wesemael, B., 2025. A framework for mapping conservation agricultural fields using optical and radar time series imagery. Remote Sensing of Environment 328, 114858.

Zhou, Y., Gómez Giménez, M., Guenet, B., de la Fuente Blanco, D., Monhonval, A., Sabetizadeh, M., Quentin, B., Heinesch, B., Longdoz, B., van Wesemael, B., under review. From Earth Observation to Carbon Farming: Quantifying Soil Carbon Sequestration in Cropland within a Monitoring, Reporting and Verification Framework. 2026. Under review.